

Bachelor's Thesis

# Development of a Sensor-Implant for Cancer Research

Niklas Fauth

Handover Date: 18.9.2019

Supervisors: M.Sc. Sebastian Meier (Texas Instruments)  
Prof. Dr. Bernhard Wolf (TUM - Steinbeis-Transferzentrum)  
Prof. Dr. Uli Lemmer (KIT - LTI)  
Prof. Dr. Andreas E. Guber (KIT - IMT)

Department of Electrical and Computer Engineering  
Karlsruhe Institute of Technology

---

Hiermit versichere ich, dass ich diese Arbeit selbstständig verfasst und keine anderen, als die angegebenen Quellen und Hilfsmittel benutzt, die wörtlich oder inhaltlich übernommenen Stellen als solche kenntlich gemacht und die Satzung des Karlsruher Instituts für Technologie zur Sicherung guter wissenschaftlicher Praxis in der jeweils gültigen Fassung beachtet habe.

Ort, Datum

Münster, der 18.9.2019

Niklas Fauth

## **Zusammenfassung**

Diese Arbeit beschreibt die Entwicklung eines Implantats, wie es in der Krebsforschung verwendet und auf industriellem Niveau produziert werden kann. Das neu entwickelte Gerät besteht aus einem embedded System welches analoge Signale von einem pH-empfindlichen Ionensensitiven Feld Effekt Transistor (ISFET)-Sensor auswertet und die Daten zur weiteren Verarbeitung über das LoRaWAN-Funkprotokoll (Long Range Wide-Area Network) an eine Basisstation überträgt. Methoden der Mikrofertigung wie HDI (High Density Interconnect)-Platten und 3D Druck durch Stereolithografie wurden eingesetzt, um einen kleinen "Button Sensor"Formfaktor von 30 mm Durchmesser und 8 mm Höhe zu erreichen. Die Elektronik wurde auf einen minimalen Energieverbrauch optimiert, um mit einer Knopfzelle eine ausreichende Batterielebensdauer zu erreichen. Die Schaltung, sowie das Gehäuseprinzip, kann als flexible Plattform für kleine drahtlose Implantate an andere Sensoren angepasst werden. Ein neuartiges, auf Lebensdauer und Miniaturisierung optimiertes PEEK Gehäuse wurde erforscht. Kombiniert mit einer O-Ring-Dichtung für die Sensoröffnung bietet es hohe Zuverlässigkeit, wie sie für medizinische Anwendungen erforderlich ist.

## **Abstract**

This thesis describes the development of an implant as it could be used for cancer research. The new device is an embedded system dedicated to reading analog signals from a pH sensitive ion-sensitive field-effect transistor (ISFET) sensor and transmitting the data to a base station for further processing via the LoRaWAN (long range wide-area network) wireless protocol. Methods of microfabrication such as HDI (High Density Interconnect) circuit boards and 3D printing by stereolithography have been used to achieve a small overall form factor. The electronic design was optimized for minimal energy consumption to achieve sufficient battery lifetime from a button cell. The circuit, as well as the package principle, can be adapted for other sensors as a flexible platform for small wireless implants. A novel PEEK housing optimized for lifetime and miniaturization has been researched. Combined with an o-ring seal for the sensor dies, it provides high reliability as required for medical applications.

## **Acknowledgments**

I would like to thank Professor Wolf for inspiring my interest in the development of sensor implants.

I would also like to express my sincere thanks to Sebastian Meier from Texas Instruments for supporting me so much. He was my first contact for questions and problems concerning the ISFET sensors and with inspiring conversations and a lot of feedback he significantly helped me in the success of this work.

# Contents

<b>1</b>	<b>Introduction</b>	<b>1</b>
1.1	Motivation . . . . .	1
1.2	Applications of this Implant Prototype . . . . .	1
<b>2</b>	<b>Introduction of the ISFET Sensor</b>	<b>2</b>
2.1	pH Concentration . . . . .	2
2.2	pH Measurement . . . . .	3
2.3	ISFET pH Sensor . . . . .	4
<b>3</b>	<b>Requirements for the Implant</b>	<b>6</b>
3.1	Medical Aspects . . . . .	6
3.2	Sensor Readout . . . . .	8
3.3	Communication . . . . .	8
3.4	Power Supply . . . . .	8
<b>4</b>	<b>Mechanical Sensor Design</b>	<b>9</b>
4.1	Gasket Design . . . . .	9
4.2	Sensor Packaging . . . . .	11
4.2.1	Flat Bond Design . . . . .	11
4.2.2	Flip Chip Design . . . . .	11
4.2.3	Future Improvements . . . . .	16
<b>5</b>	<b>Implant Electronics Design</b>	<b>17</b>
5.1	System Overview . . . . .	17
5.2	Battery and Power . . . . .	18
5.3	Multi-PCB Integration . . . . .	19
5.4	Communication . . . . .	21
5.4.1	Antenna Design . . . . .	21
5.4.2	Transceiver Selection . . . . .	25
5.4.3	Transceiver Design . . . . .	27
5.4.4	Antenna Matching . . . . .	27
5.5	Sensor Readout Circuit . . . . .	29
5.5.1	Analog Front-End . . . . .	29
5.5.2	Electrode Subsystem . . . . .	32
5.6	PCB Layout . . . . .	34
<b>6</b>	<b>Firmware and Software</b>	<b>35</b>
6.1	Implant Firmware . . . . .	35
6.1.1	Radio Initialisation . . . . .	35
6.1.2	Theory of Operation . . . . .	36
6.2	Server-side Software . . . . .	37
<b>7</b>	<b>Implant Tests and Results</b>	<b>37</b>
7.1	LoRa Range Test . . . . .	37
7.2	Power Consumption . . . . .	38
7.3	Leakage Test . . . . .	40
7.4	Sensor Implant Operation Test . . . . .	42



# List of Figures

1	Schematic representation of MOSFET (left) and ISFET (right) typical structures.	4
2	ISFET sensor die (right), next to a commercial flipchip IC with 0.5 mm ball pitch (left).	5
3	SEM-photo shows RT112 cells on a ISFET.	6
4	Light-microscope photo shows a complete monolayer of RT112-cells on an ISFET-sensor chip.	6
5	Conceptual presentation of an application for the implant.	7
6	ISFET die in CLCC package (left: sealed with grey epoxy glue)	9
7	ISFET die bonded to a PCB, sealed with clear epoxy glue.	9
8	System Overview	10
9	O-ring inside 1.3 mm PCB hole.	12
10	O-ring as seen from the top.	12
11	Testing the Solderability.	13
12	ISFET die with gold studbumps applied to the bondpads.	13
13	Overview of the sensor packaging process.	14
14	Stainless steel stencil with nine different alignment designs.	15
15	Aligned stencil without the ISFET sensor.	15
16	Sensor placed in stencil, ready for soldering.	15
17	Cross-section of the assembled implant.	16
18	System Overview	17
19	Comparison of internal structure for single sensor and dual sensor implant.	19
20	PCB rings used for connecting the lower ISEFT sensor.	20
21	Exploded view of electronics.	20
22	The attenuation constants for various parts of the human body.	21
23	Different (PCB) antenna designs evaluated by Silicon Labs	22
24	Silicon Labs Panic Button ILA	22
25	3D model and Farfield Analysis of the PCB antenna assembly in CST Studio	23
26	Measuring antenna parameters in as assembled implant buried in pork.	24
27	Return loss of the unmatched PCB antenna.	24
28	Smith chart of the unmatched PCB antenna.	24
29	Laird Sentrius™ Indoor Gateway.	26
30	Outdoor LoRaWAN to 3G Gateway for remote applications.	26
31	Section of the implants schematic shows the LoRa transceiver circuit.	27
32	Circuit of a PI matching network.	27
33	Traditional ISFET bridge-type readout circuit.	29
34	Section of the implants schematic shows one of the two AFE + MUX	30
35	Section of the implants schematic shows the electrode control.	32
36	Screenshot of the mainboard PCB Layout. Copper pours are deactivated to show the inner traces.	34
37	Three assembled mainboards.	34
38	Screenshot of the sensor PCBs Layout. Left: Lower sensor PCB. Right: Upper sensor PCB with LoRa antenna	34
39	Time sequence of the implant functions.	36
40	RSSI over distance for both tests.	38
41	Extrapolated battery lifetime over sample rate.	39
42	Implant holder with microfluidic attachment.	40
43	Measurement setup. Right is fresh electrolyte, left is waste water.	40

44	Leakage current of two implant versions in comparison. . . . .	41
45	Implant in test solution after 10 min. . . . .	42
46	Implant in test solution after 60 min. . . . .	42
47	Differential pH as measured by the implant over time. . . . .	43
48	Assembled implant with mainboard sensor PCB, 1 Euro coin for size reference.	44

## List of Abbreviations

<b>pH</b>	A scale for the concentration of hydrogen ions in a solution.
<b>MOSFET</b>	Metal-Oxide-Semiconductor Field-Effect Transistor
<b>ISFET</b>	Ion-Sensitive Field-Effect Transistor
<b>REFFET</b>	Reference Field-Effect Transistor
<b>USP Class</b>	Classification for medical devices by the United States Pharmacopeia
<b>TÜV</b>	Technischer Überwachungsverein
<b>IP67</b>	International Protection Marking, Dust tight & Immersion, up to 1 m depth
<b>PCB</b>	Printed Circuit Board
<b>HASL</b>	Hot Air Solder Leveling, a common PCB surface finish
<b>FR4</b>	flame retardant - 4, a common epoxy-based PCB material
<b>SMD</b>	Surface-Mounted Device
<b>HDI</b>	High Density Interconnect
<b>IC</b>	Integrated Circuit
<b>COB</b>	Chip On Board
<b>CSP</b>	Chip Scale Package
<b>CLCC</b>	Ceramic Leadless Chip Carrier
<b>PEEK</b>	Polyether Ether Ketone
<b>LPCVD</b>	Low Pressure Chemical Vapor Deposition
<b>CNC</b>	Numerical Control
<b>CAD</b>	Computer-aided design
<b>SLA</b>	Stereolithography Apparatus
<b>SEM</b>	Scanning Electron Microscope

<b>CPU</b>	Central Processing Unit
<b>MCU</b>	Microcontroller Unit
<b>STM32</b>	32 bit ARM™ Microcontroller Series by STMicroelectronics
<b>ADC</b>	Analog-to-Digital Converter
<b>DAC</b>	Digital-to-Analog Converter
<b>SPI</b>	Serial Peripheral Interface
<b>AFE</b>	Analog Front-End
<b>OP</b>	Operational Amplifier
<b>MUX</b>	(analog) Multiplexer
<b>LSB</b>	Least Significant Bit
<b>DC</b>	Direct Current
<b>RF</b>	Radio frequency
<b>CV</b>	Constant Voltage
<b>CC</b>	Constant Current
<b>CCCV</b>	Constant Current Constant Voltage
<b>VDD</b>	Voltage at Drain, usually referenced to as the positive supply voltage
<b>VSS</b>	Voltage at Source, usually referenced to as the negative supply voltage
<b>GND</b>	Ground, usually referenced to as a local 0 V potential.
<b>LoRa</b>	Long Range
<b>LoRaWAN</b>	Long Range Wide-Area Network
<b>GPS</b>	Global Positioning System
<b>NFC</b>	Near-Field Communication
<b>WiFi</b>	Trademarked phrase referring to IEEE 802.11x
<b>MICS</b>	Medical Implant Communication Service
<b>ISM</b>	Industrial, Scientific and Medical radio bands
<b>SRD</b>	Short-Range Device
<b>IoT</b>	Internet of Things
<b>GCC</b>	GNU Compiler Collection
<b>LAN</b>	Local Area Network
<b>LXI</b>	LAN eXtensions for Instrumentation
<b>TCP/IP</b>	Transmission Control Protocol / Internet Protocol
<b>MQTT</b>	Message Queuing Telemetry Transport
<b>RX</b>	Receive
<b>TX</b>	Transmit
<b>BW</b>	Bandwidth
<b>VSWR</b>	Voltage Standing Wave Ratio
<b>RSSI</b>	Received Signal Strength Indicator
<b>ILA</b>	Inverted L Antenna
<b>VNA</b>	Vector Network Analyzer
<b>LPF</b>	Low-Pass Filter

# 1 Introduction

## 1.1 Motivation

One of the key challenges of modern cancer research is understanding the effects of various treatments on cancer cells in tumors. Accelerating the observation of both positive and negative reaction of cancer cells is important for research, but also to find the right treatment for an individual patient and improve the diagnose. One way of this in-vivo observation is measuring the pH and O<sub>2</sub> value of cells of the tumor, as these parameters reflect the health of the tissue in question.[1]

The feasibility of this measurement highly depends on the availability of small and long-term stable electrochemical sensors. As the sensor needs to be in close proximity to the cancerous tissue inside the living organism, an wireless implant has to include all necessary peripherals such as a battery and communications. To make the implant as small as possible to improve comfort and to reduce harm on healthy tissue, state of the art micro-fabrication techniques such as HDI (High Density Interconnect) circuit boards are necessary.

This thesis evaluates the feasibility of such an implant, design choices made and the challenges faced during development and manufacturing of the finished implant. It is structured as follows: In the first section, an overview is given on the ion sensitive field effect transistor (ISFET). Next, the second section explains the process of investigating an ideal packaging option for the ISFET sensor. The third section deals with the electronics developed for this implant. The implant is then tested and verified in the forth section. Finally, the last section gives an outlook on what measures have to be taken so that this conceptual sensor can be fabricated on large scale, and pass according to requirements of USP Class VI for medical implant devices.

## 1.2 Applications of this Implant Prototype

This implant was developed in cooperation with Texas Instruments, which made the ISFET sensor and provided engineering samples, and the Steinbeis-Transferzentrum for Medical Electronics and Lab on Chip-Systems<sup>1</sup>, supervised by Prof. Dr. Bernhard Wolf. Areas of research include systems for systemic drug discovery and tumor diagnosis and treatment.

This already includes possible applications this implant is developed for. Being able to measure the local health of tissue in real-time, the implant allows much faster information on success of a specific drug or treatment than it would be possible by eg. biopsy:

For the area of drug discovery and research, this is valuable in animal experiments, where a artificially induced tumor can be monitored to test it's reaction to novel substances.

For cancer treatment on humans, similar applications are imaginable. Especially for types of cancers with a high mortality rate or high risk of recurrence, monitoring the patient after surgery is crucial to decide on further therapy. After surgical removal of a tumor, the implant could be used to monitor the affected tissue[2].

This also becomes relevant for certain chemotherapies with the risk of drug resistance, eg. for metastatic breast cancer. "The subsequent development of drug resistance can result in rapid

---

<sup>1</sup>Website of Steinbeis-Transferzentrum for Medical Electronics and Lab on Chip-Systems: <http://stw-med-chip.de/>

disease progression during or shortly after completion of treatment" [3]. Monitoring cancer in such a direct way might be a chance for predicting better therapies and adjusting them based on the data available through the implant.

Another application of a future version of this implant might even involve direct treatment of the tumor. Not only can the pH value around the tumor be measured, it can also be actively changed, with significant effects on growth rate [4]. One simple way of changing the local pH value would be using the platinum electrodes of the ISFET sensor to induce a electrical current in the tissue, consuming H<sup>+</sup> cations or OH<sup>-</sup> anions around the electrodes. This causes an increase of the pH value around the cathode (more basic) or an decrease of the pH value around the anode (more acidic).

## 2 Introduction of the ISFET Sensor

### 2.1 pH Concentration

Hydrogen potential, known as pH, is a measure of the chemical activity of hydrogen ions in solution. In aqueous solution, these ions are present in the form of hydronium ions.

pH is a scale used to specify the acidity or basicity of a solution.

- a solution of pH = 7 is said to be neutral;
- a solution with a pH < 7 is called acidic. The lower its pH, the more acidic it is;
- a solution with a pH > 7 is called basic. The higher its pH, the more basic it is.

For diluted solutions, the pH value approximately corresponds to the mass concentration  $c$  of the hydroniu ions ( $\text{H}_3\text{O}^+$ ) in mol per litre (with  $c^\circ = 1 \text{ mol per litre}$ ) [5]:

$$\text{pH} = -\log_{10} \left( \frac{c(\text{H}_3\text{O}^+)}{c^\circ} \right) \quad (2.1)$$

The pH value plays an important role in many areas of everyday life, for example in detergents or the taste of lemonade.

Also in the body, the pH value is of great importance for metabolic reactions and healthy cell growth. A distinction is made between intracellular (pHi) and extracellular pH (pHe). The pH value can vary depending on the type of tissue and state of health. Thus, the measurement of pH is a possible indicator for cancer diagnosis and therapy. "The pHe of the tumor microenvironment is typically acidic, in the range of 6.5 to 6.9, whereas the pHe of normal tissue is approximately 7.2 to 7.5." [6]

The pH can also have an influence on the success of a therapy: "That the pH of the cellular environment might influence the effectiveness of various therapeutic agents is not a new idea." [7]

## 2.2 pH Measurement

Today, a variety of pH sensors are available on the market. Most of them require a reference electrode, which has a constant voltage potential in reference to the electrolyte under test.

All potentiometric pH measurement methods are based on the Nernst Equation. It describes the electrical potential of an electrochemical cell as a function of concentrations of ions.

$$E = E_0 - \frac{RT}{nF} \ln(Q) \quad (2.2)$$

With  $E$  being the resulting potential,  $E_0$  being the standard half-cell reduction potential,  $n$  being the number of electrons exchanged and  $Q$  being a reaction quotient (relative amounts of products and reactants present in the reaction). In practice this equation is often further simplified by using a conversion factor between natural logarithm and decimal logarithm.  $RT/F$  is constant for a given temperature, resulting in a constant factor of 0.0591 for 25°C.

This dependency is exploited by the most common pH sensor, the glass electrode. It is made of a doped glass membrane that is sensitive to a specific ion. The electrode is filled with an electrolyte of pH = 7. If combined with a reference electrode that has pH-independant potential, the cell voltage corresponds to the pH concentration as given by Nernst Equation:

$$E = E_0 + 0.0591 \log \left( \frac{[\text{H}^+_{\text{inside}}]}{[\text{H}^+_{\text{outside}}]} \right) \quad (2.3)$$

Using the definition of pH ([Equation 2.1](#)):

$$E = E_0 + 0.0591 (\text{pH}_{\text{outside}} - \text{pH}_{\text{inside}}) \quad (2.4)$$

There are multiple disadvantages that come with glass-based discrete pH sensitive electrodes. Because of the complex glassware involved with building even small glass electrodes, manufacturing costs are high. They are usually only available as complete discrete elements that are hard to integrate in small formfactors, i.e. non applicable for implants. Additionally the impedance of such electrodes is very high, in the range of 100 MΩ - 1 GΩ. Precision amplifiers with very low leakage current suitable for glass electrodes are expensive and require high quiescent current.

Other disadvantages of this method include large size and thus high costs associated with the reference electrode, which up until today has not been integratable / miniaturizable in a long-term stable fashion.

Another notable approach to measuring the pH concentration are metal - metal oxide pH sensitive electrodes, which have been shown not to be stable for a long term and have problems associated with noise, as well as drift, hysteresis, and chemical (surface) stability.

## 2.3 ISFET pH Sensor

A more suitable method of measuring pH value in a solution is the usage of an ISFET (Ion-Sensitive Field-Effect Transistor) as the ion-sensing element. In case of the ISFET provided by Texas Instruments, the electrode material is LPCVD (Low Pressure Chemical Vapor Deposition) Si<sub>3</sub>N<sub>4</sub>. These components also require a reference electrode to perform absolute pH measurement. However, if operated standalone, ISFETs can still provide a small and cheap differential pH sensing solution.

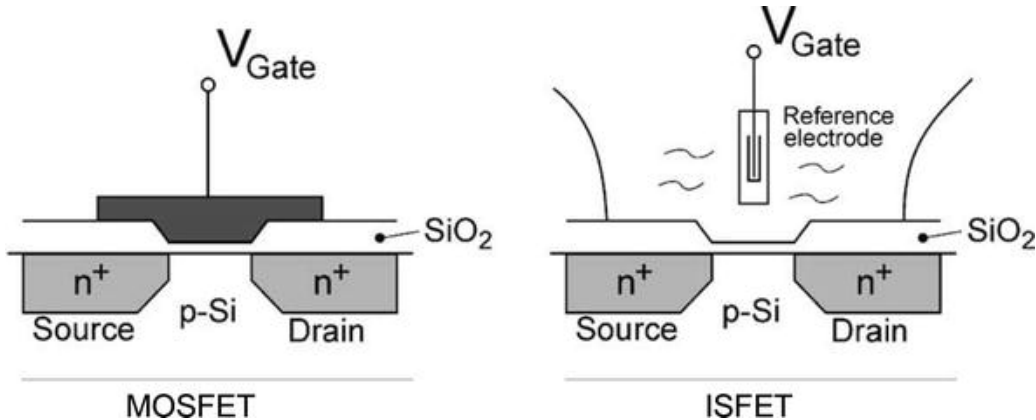


Figure 1: Schematic representation of MOSFET (left) and ISFET (right) typical structures. Illustration taken from "Transistors as an Emerging Platform for Portable Amplified Biodetection in Preventive Personalized Point-of-Care Testing" [8]

The ISFET, developed by Bergveld in 1970 [9], relies on the fact that dielectrics have surface charge effects that are pH sensitive, which can be amplified by a field effect transistor. The transistor can be seen as a transimpedance amplifier, resulting in a much lower impedance compared to glass electrodes.

An ISFET is comparable in function to a common MOSFET. While for MOSFETs, the gate-source threshold voltage  $U_{GS(Th)}$  is constant under stable operation conditions, for ISFETs,  $U_{GS(Th)}$  changes accordingly with the activity of ions in the chemical solution by charge modification of potential across semiconductor-dielectric-electrolyte interface. Since this effect also follows laws of Nernst Equation, the maximum achievable change in  $U_{GS(Th)}$  per pH step is 59 mV/pH (Nernst limit). In reality, the sensitivity of the ISFET is reduced by a factor  $\alpha$ . The ISFETs provided by Texas Instruments show a sensitivity of 57 mV/pH.

The implant has to be built in a way that allows this ion-sensitive gate isolator to get immediate (<1mm) proximity to the cancerous tissue, i.e. the electrolyte under test. An external electrode is used to control the liquid potential (liquid gating).

In order to only measure the change of ion concentration, all other parameters that have an effect on the threshold voltage, like temperature or long-time drift, must be controlled or compensated. Most of non-linear distortion effects can be eliminated by operating the ISFET at a constant drain-source voltage and current (CVCC). In order to compensate for external factors like temperature, a reference MOSFET (REFFET, Reference Field-Effect Transistor) with same electrical properties as the ISFET, located on the same die so it is exposed to similar environmental effects as the actual ISFET, can be used as a non pH-sensitive reference.

The ISFET sensor used in this thesis was fabricated by Texas Instruments in Freising, Germany,

2019. It contains 4 different ISFET designs, 4 complementary REFFETs and two platinum electrode structures.

The smaller, inner electrode directly surrounds the four individual ISFET gates and is used to apply the gate control voltage.

The outer, square electrode has a slightly larger distance to the gates and surrounds both the ISFETs and the REFFETs, visible in [Figure 2](#), with a size of 1 x 1 mm.

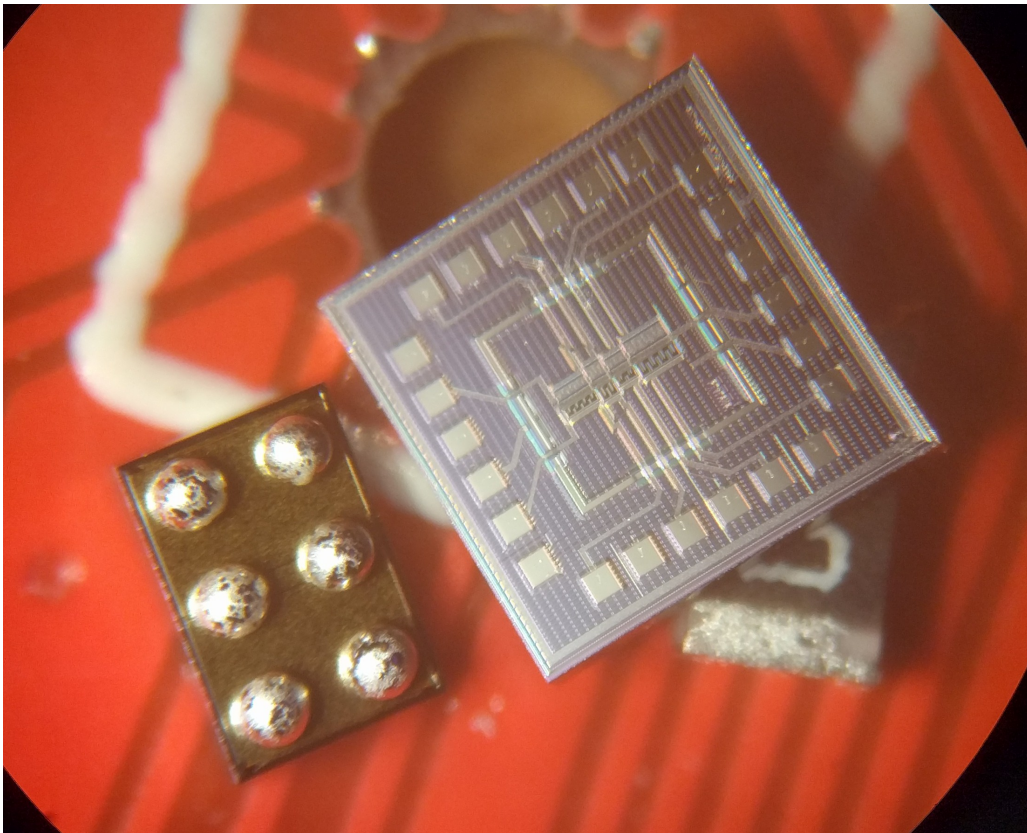


Figure 2: ISFET sensor die (right), next to a commercial flipchip IC with 0.5 mm ball pitch (left). Photo created by author

The sensor die was originally designed for low cost, and is one of many so-called "zebras", i.e. contains studies on ISFET geometry, the outcome which will be published elsewhere. Thus, to get a high number of experiments made per wafer, each die only measures 2 x 2 mm in size. Handling of these small dies is a challenge. For development purposes, ISFET dies are typically glued inside an off-the-shelf ceramic leadless chip carrier (CLCC), where it is bonded and sealed with epoxy glue. While this allows easy further usage of the sensor, this packaging method does not meet the size requirements of this implant. Instead, a new packaging option was required that connects and mounts the sensor die within the limited space.

In order for the ISFET to operate properly, the sensing area has to be in contact with the liquid to be measured.

While this area has to be exposed to the outside, all the connections and electronics around this area have to be sealed to prevent leakage and electrical shorts. Even a small amount of moisture could damage the sensitive electronics and reduce lifetime of the implant.

## 3 Requirements for the Implant

### 3.1 Medical Aspects

Given the fact that the implant is supposed to be implanted into a living being at some point, some special requirements have to be satisfied to ensure reliability and patient safety. While in this thesis, the implant to be developed is considered a prototype that is never to be used inside a human, development was done with use as a medical device in mind. This makes it easier for further development to pass TÜV test to allow tests with animals.

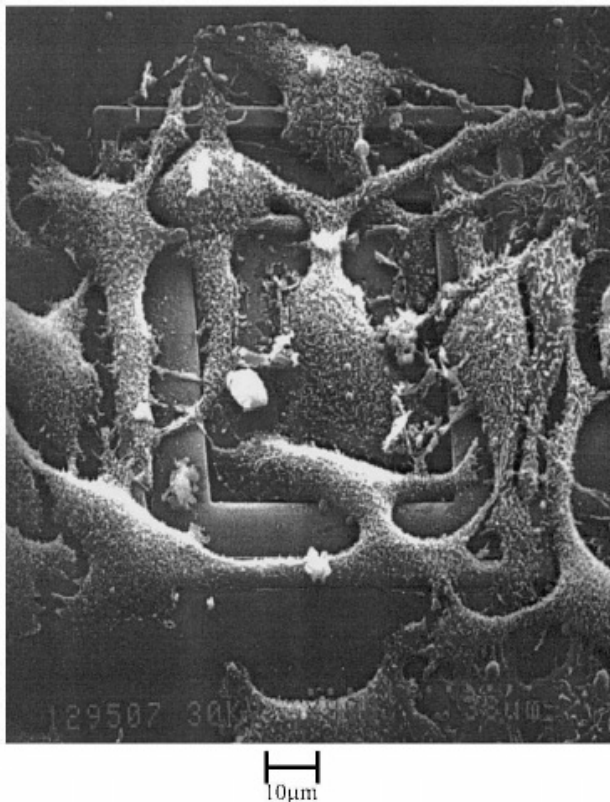


Figure 3: "The SEM-photo shows RT112 cells on a ISFET."

Figure taken from “Microelectronic sensor system for microphysiological applicationon living cells”[\[2\]](#)

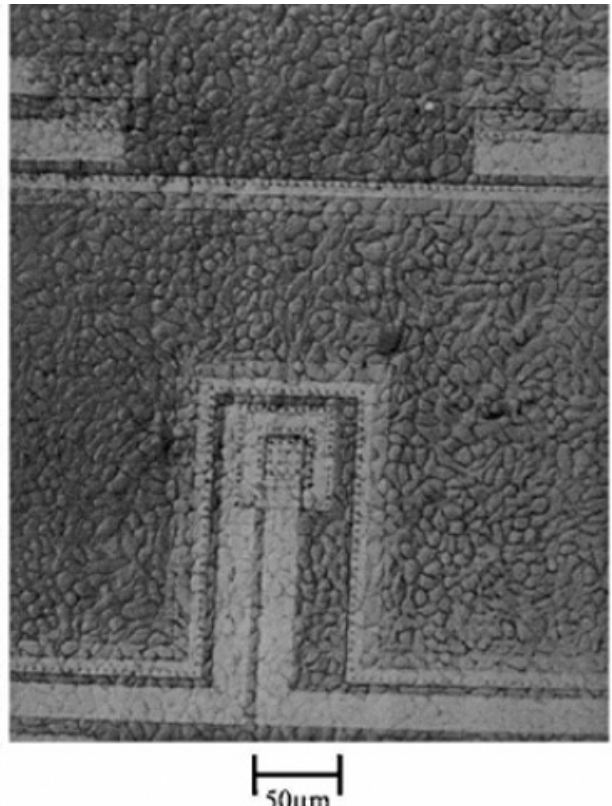


Figure 4: "The light-microscope photo shows a complete monolayer of RT112-cells on an ISFET-sensor chip." Figure taken from “Microelectronic sensor system for microphysiological applicationon living cells”[\[2\]](#)

The sensing area of the implant is supposed to be in close proximity to the cancerous tissue of the tumor, with cancer cell size range from 10 μm to 100 μm. For eg. pancreatic cancer and other internal types of cancer, this requires a complex surgical procedure. To damage as few healthy tissue as possible, an overall small form factor is preferred. To ensure good contact with the tissue of interest, a flat, button-like form factor turned out to be most promising for easy and reliable application. Fastening eyelets around the side of the implant can be used to sew the sensor in place.

Once installed, the implant is supposed to stay inside the patient, so in case of a successful therapy, no additional operations to remove the implant are required. This also enables possibilities for long-term monitoring of the patient after therapy.

This requirement is relevant especially for the case of the implant, as well as power delivery and communication. In order to minimize the damage for healthy tissue, the implant should be small in volume. To ensure good biocompatibility, PEEK (Polyether ether ketone), which is suitable as a chemically resistant construction material, was used for the outer sensor package. All other material in contact with tissue have to pass medical implant requirements according to USP Class VI.

With the implant being buried deep inside the body (5 - 20 cm in case of the pancreas, for humans[10]), wired power and communication is not an option. Wireless operation is necessary to get data from the implant.

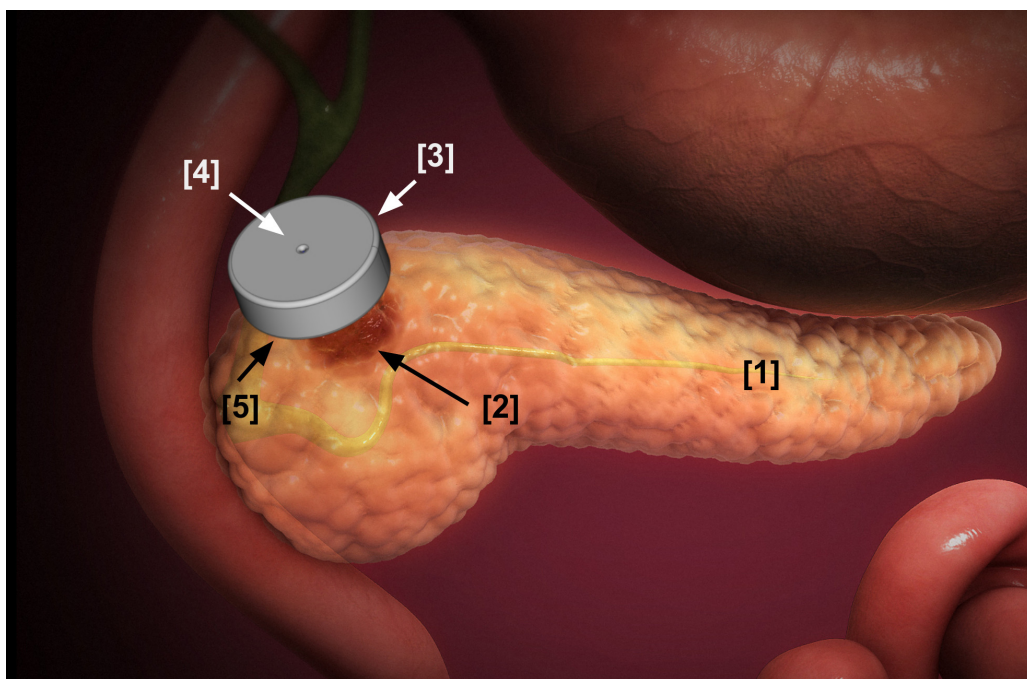


Figure 5: Conceptual presentation of an application for the implant. <sup>2</sup>

- [1] Pancreas
- [2] Tumor tissue
- [3] Sensor implant
- [4] Opening for differential reference-ISFET
- [5] (faced backwards) Opening for primary ISFET

Instead of getting an absolute reading on the pH value of the cancerous tissue, pH value is measured in reference to healthy tissue (Figure 5). This removes the need of a reference electrode, and simplifies the design as instead of two different parts have to be in contact with the tissue, the sealing concept developed for the ISFET sensor can be used for both openings of the implant.

<sup>2</sup>Scientific Animations Inc., *Pancreatic cancer*,  
<http://www.scientificanimations.com/wiki-images/>

Modified by author as permitted by the Creative Commons Attribution-Share Alike 4.0 International License,  
 Jan. 2018

### 3.2 Sensor Readout

As the sensor IC used for this implant is supplied as a bare die with ISFETs as only active circuitry, additional analog electronics is required to get useful data from the sensor. The gate-threshold voltage  $U_{GS}$  has to be measured at stable conditions, thus operating the ISFET in the linear range is preferred. To achieve this, a constant current  $I_{DS}$  and a constant voltage  $U_{DS}$  (CCCV) is necessary. As the gate reference voltage applied to the solution has to be the same for both ISFETs, this voltage can't be changed relative to battery ground of the implant as different reference voltages for the individual ISFETs would cause a current flowing from one side of the implant to the other. Thus, the whole ISFET has to be floating in order to swing according to the changing  $U_{GS}$ , and so does the circuit that provides the CCCV. Ideally the parameters of operation, like  $I_{DS}$  and  $U_{GS}$ , can be adjusted later in software.

To compensate for long-term distortions like temperature change and drift effects, the REFFET complementary to the ISFET on the same die can be used as a reference. For the REFFET to match the characteristics of the ISFET, identical operation conditions have to be ensured. Because the REFFET and ISFET of one sensor die share a common source, the circuit for the constant current source of the REFFET also has to be floating. In conclusion, the implant must include four precise, programmable constant current, constant voltage sources that are small in size and require as little power as possible.

### 3.3 Communication

In order to access the measurement results from the implant, some wireless communication must be implemented to extract data. Popular solutions for this are magnetic low-frequency transponders. This might be suitable for use with humans, as a suitable reader, like a smartphone with NFC, can be placed at controlled times of the day near the patient.

As this implant is planned to be employed in animal studies, it is more conveniently and reliable to extend the range to at least 5m from the subject. This allows a single receiver unit to be used in a facility that accommodates multiple test animals.

### 3.4 Power Supply

There are multiple options for wireless power supply. The main three concepts already being used for such applications are:

- Wireless power transfer using inductive coupling [12]
- Wireless power transfer for charging an internal battery [13]
- Internal non-rechargeable battery [14]

The main advantage of the first two option is the basically unlimited battery lifetime. Unfortunately, these rely on some way of transmitting sufficient wireless power (ca. 100mW) far enough inside the body. This is only possible with good inductive coupling, which requires big coils or strong fields. Both is inapplicable for the implant to be designed in this thesis.

The only option left is using a non-rechargeable battery, and drawing as little power as necessary to get the best possible battery lifetime.

A typical study on both animals and humans usually takes no longer than 90 days. This is the minimum battery lifetime that must be achieved after activation of the implant. A rough estimation of the worst case power consumption, using the datasheet specifications on power consumption of the used ICs, results in an average power consumption of 3 mW during active measurement and 100mW during data transmission. The measurement rate can be fairly low, as biological processes of this scale happen in the matter of hours. With an estimated standby power consumption of 100 uW and a duty cycle of 1% for measurement (< 1 second of measurement every minute) and 0.1% for the radio, this results in a required battery capacity of

$$(3mW * 0.01 + 100mW * 0.001 + 0.1mW * 0.989) * 90d * 24h = 0.44Wh \quad (3.1)$$

This will was used as a reference for selecting a suitable battery.

## 4 Mechanical Sensor Design

### 4.1 Gasket Design

Sealing and packaging the sensor die is one of the key challenges during development of a reliable implant. The main issue here is to make sure the ISFET's sensitive area is in contact with the tissue around the implant, while the electrical contacts and circuit, just 500  $\mu\text{m}$  beside, stays dry, even after prolonged exposure to the aggressive environment inside the body.

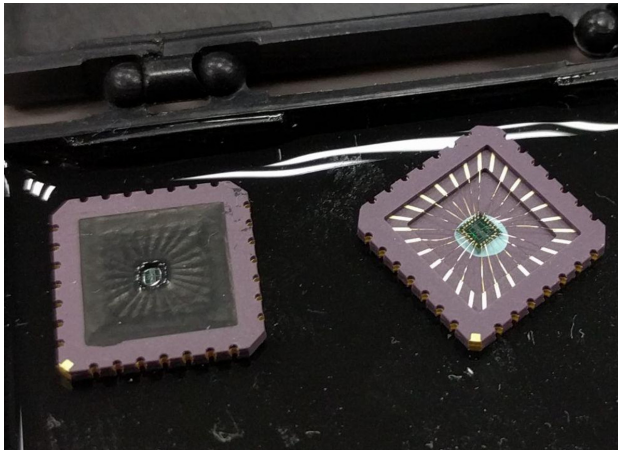


Figure 6: ISFET die in CLCC package (left: sealed with epoxy glue). Photo created by author for a previous work.

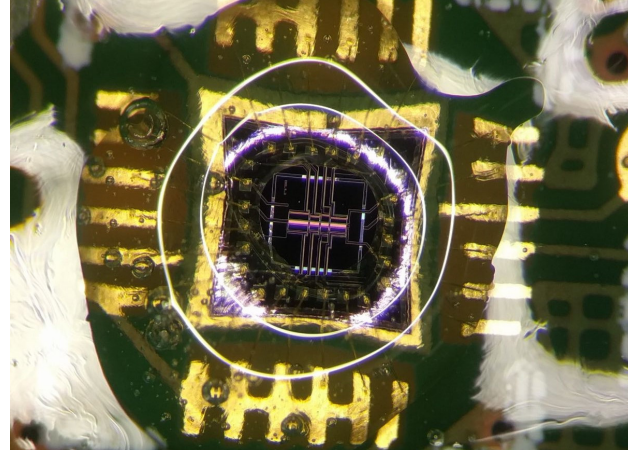


Figure 7: ISFET die bonded to a PCB, sealed with epoxy glue. Photo created by author for a previous work.

From earlier experiments performed at Texas Instruments with packaging methods involving epoxy glue for sealing the ISFET sensor, it has been shown that this method is unreliable for long-time tightness. Water creeps in at the interface between epoxy and silicon, wetting the bond pads and causing leakage current. This happens within the scale of hours to days, too short as an option for an implant.

The reasons for adhesion loss at high relative humidity are not fully understood. Suggested causes include degrading of polymer chains at the interface, and swelling of polymeric material, creating tension that causes micro cracks, letting water soak deeper into the epoxy. [15].

Another problem with using glues comes with the very principle of how glues work. In order to be applied liquid and later hardened to be a solid, both single and dual compound glues contain chemicals that are present in some sort of ionic solution, e.g. in acidic form. Even if processed as per manufacturer's specifications, unreacted compounds can leak ions into the measurement solution.

A different sealing method is required for this thesis, made of a material that prevents mechanical degradation by being elastic and resident to water. Ideally, this seal would be located in between the PEEK housing and the ISFET sensor to avoid additional transitions and thus possible error points.

To test various options, multiple O-rings have been ordered from "Apple Rubber". The different O-rings are made from either Fluorocarbon or Silicone and vary in size, with all being small enough to fit on the sensitive area of the ISFET sensor die.

Overview of evaluated O-ring properties					
OD (mm)	ID (mm)	CS (mm)	Material	Shore A	Color
1.40	0.74	0.33	Fluorocarbon	75	Black
1.33	0.61	0.36	Fluorosilicone	70	Blue
1.32	0.50	0.41	Medical Grade Silicone	80	Clear
1.13	0.53	0.30	Silicone	60	Red
1.06	0.46	0.30	Fluorocarbon	75	Black

This selection of O-rings was helpful to adjust the seal to the requirements such as tightness and fit. All five O-rings have been tested with an individually designed case. While the rings with smaller outer diameters are in favor regarding ease of assembly and packaging the ISFET as there is more space towards the bond pads, these rings have the problem that due to the small cross section the surface of the ISFET is not properly wetted. The most promising O-rings are the blue 1.33 mm OD and the black 1.40 mm ring.

Using an O-ring as the primary seal between measurement solution and electronics solves the issues epoxy glue would introduce: It is flexible and thus cannot crack or lose contact, and because it is made as a separate part, the manufacturing process can involve steps like tempering at high pressure / temperature (e.g. rubber vulcanization), creating a material that is much more resistance to chemicals and has good pH neutrality.

One main issue that comes with using O-rings is mechanical engineering of the gasket: While glue is straightforward to use, the O-ring requires a more sophisticated approach. It needs a well engineered interface that holds it in place reliably and applies a defined pressure to compress the ring by 25% as required by the manufacturer.

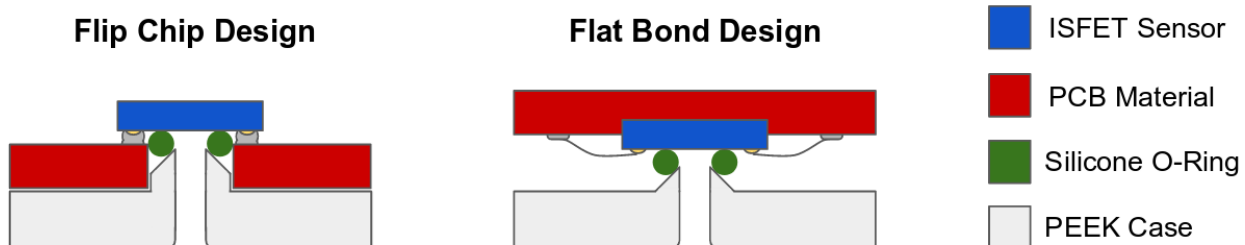


Figure 8: O-ring design concepts. Illustration created by author

Two concepts were developed for how the O-ring could be installed in the implant. Both are based on the idea that the O-ring rests flat on the ISFET sensor and is pressed and centred through a concentric mandrel with chamfer in the PEEK housing of the implant. Since the opening for the ISFET sensor is located exactly in the middle of the respective round housing, such a structure can easily be produced with a CNC (Numerical Control) lathe.

For prototyping purposes, the case was designed in 3D using CAD (Computer-Aided Design) and 3D printed using an Anycubic Photon stereolithographic (SLA) printer. This way, multiple versions of the case can be rapidly prototyped and evaluated. This is particularly useful for iteratively improving the o-ring interfaces, as small changes in geometry can improve the ease of alignment and sealing.

## 4.2 Sensor Packaging

The main difference between the O-ring design concepts is the way the ISFET die is packaged. In the left design in [Figure 8](#), the die is soldered onto a circuit board, with the die being "upside down" relative to the PCB. Hence the name "flip chip design". In the right example, the die is embedded with die attach into a pocket milled into the PCB, with electrical connections bonded to the PCB using a standard wirebond process.

### 4.2.1 Flat Bond Design

The flat bond design was evaluated first, as it is very similar to the CCLC packaging process. Bonding the die onto a PCB instead of into a ceramic carrier is a well established industry standard process called COB (chip on board). A pocket was milled into the PCB for the ISFET to have the die at a defined position which helps with later aligning the O-ring. This also makes the design more flat. The experiment seen in [Figure 7](#) was manufactured this way. For the implant, the epoxy glue would be replaced by the O-ring interface.

While this method was tested successfully for an evaluation design, it was not used for development of the implant. The main difficulty with this design proofed to be the alignment of the O-ring in the chip. For the O-ring to self-align on the mandrel of the housing, it needs to be precisely aligned on the ISFET. Also, this design is less space efficient than the flip chip design, as it created a pocket between the case and the sensor PCB that can't be used for anything else.

Another consideration against this attempt and for the flip chip design is the suitability for mass production. In mass production, bonding the chip to the PCB is a time-expensive step. Soldering an IC in a chip scale package is a cheap process used for nearly every modern electronics device.

### 4.2.2 Flip Chip Design

With the ISFET die being mounted with the sensitive area facing onto the sensor PCB, the O-ring can be mounted in a plane with the sensor circuit board. Using a hole in the board that matches the outer diameter of the O-ring, the ring is precisely aligned on the ISFET by simply dropping it into this hole.

Because the O-ring is in plane with the PCB, it does not add up on total height of this assembly. Through the height of PCB + die is the same as with the flip chip design, this way it does not create a hollow pocket and the space around the ISFET die can be used to give room to components mounted on the mainboard.

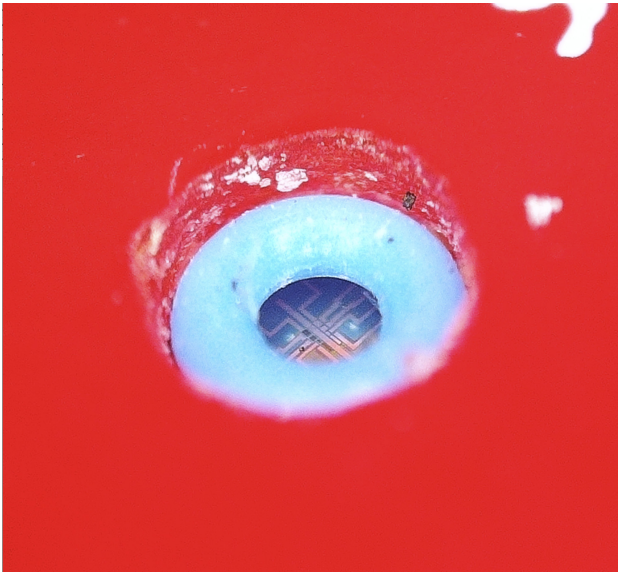


Figure 9: Blue fluorosilicone O-ring inside 1.3 mm PCB hole.

Aligned on the soldered-on ISFET and ready to be mounted in the housing.

Photo created by author.



Figure 10: Black fluoroelastomer O-ring as seen from the side where the die would be located, as indicated by the white rectangle on the PCB. The ISFET was replaced with a glued-on piece of glass for purpose of leak-proof tests.

Photo created by author.

The difficulty that comes with the currently available ISFET die is that it was not intended to be packaged in this way. Because it was made to be packaged in CLCC packages, never meant to be soldered to directly, its bond pads are small, with a pad to pad pitch of only 220  $\mu\text{m}$ . The surface of the pads is made of platinum which is generally considered solderable, still it is not suitable for direct soldering. The surface is too smooth to be well wetted by solder.

In order to reliably solder the chip onto a PCB, it is important to ensure the solder creates a strong bond with the bond pad surface. Multiple things have been tried to improve the solderability. It was known from earlier experiments with older chip generations that a rough platinum surface improves solderability. However the platinum surface is not only exposed at the bond pads, but is also used for the electrode and FET structures of the chip, where a bad surface quality had negative influence on stability and lifetime.

One way of achieving both a good surface quality for the ISFET and good solderability on the bond pads is to process the wafer for best surface quality, and then to mask the inner electrode structure. Treating the exposed bond pads with piranha solution can roughen the platinum surface. This was tried without covering the sensitive area, just to find out if this method generally works, by placing diced ISFET dies in piranha solution for 5 min, resulting in an estimated etch depth of 10 - 15 nm [16]. To test the solderability, solder paste was placed onto

the ISFET die and heated to 280 °C. If the bond pads are easily wetted by the solder, it can be expected that they also solder reliably onto the PCB, using the same paste and temperature. In case of an unprocessed sensor die, no solder at all sticks to the platinum surface, with little chance of a reliable solder joint to the PCB, as depicted in [Figure 11](#).

Roughening the surface with piranha did improve the solderability, but not as well as expected for a reliable soldered joint. Also, this method would have either required a new mask to cover the sensitive area of the ISFET with a protection layer while etching, or would be labour intensive if this protection would be applied by hand.

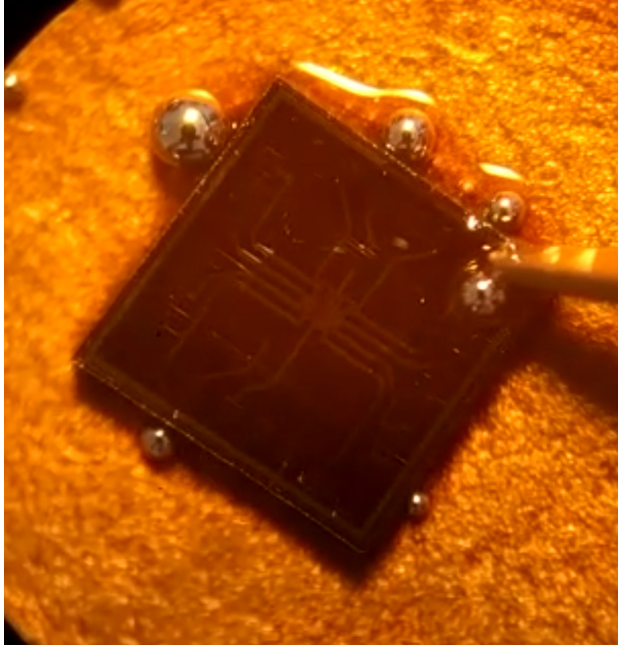


Figure 11: Testing the Solderability. After melding the solder paste, no solder sticks to the bondpads. Photo created by author.

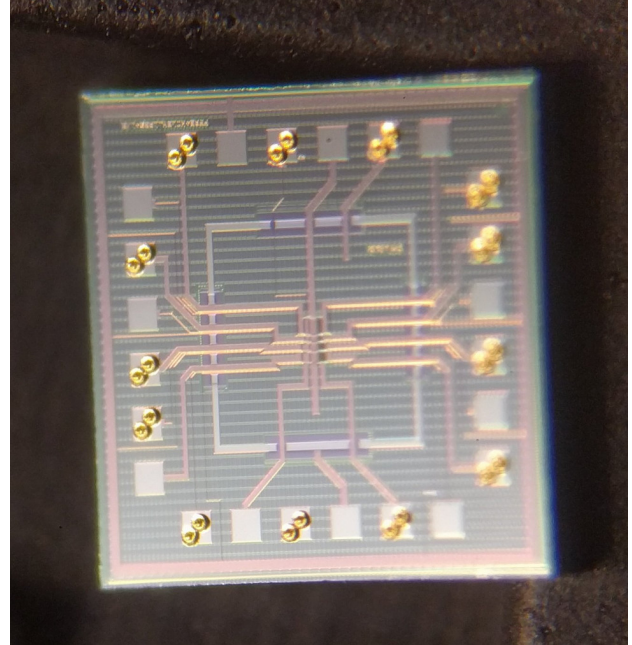


Figure 12: ISFET die with gold studbumps applied to the bondpads using a wirebonder. Photo created by author.

Another, more promising solution has been tested: Applying gold studbumps using a wirebonder (see [Figure 12](#)). A small amount of gold wire is ultrasonically welded to the bond pads, enough to provide good solderable contact area for the solder paste. This process can be applied to already processed dies or even whole wafers without requiring expensive tooling like a new mask, so this process was easy to prototype.

Another challenge is the pad pitch of 220 µm. Typical solder ball pitches for commercial wafer-level chip scale packages are 350 µm, 400 µm and 500 µm [17]. Advantageously, only every second pin of the ISFET sensor is required for this application. By only connecting required pins, this increases the effective pitch to 440 µm. Only at one point two adjacent pads have to be contacted. While small balls reduce the risk of short-circuits, unevenness in the circuit board surface can be compensated less effectively. The best compromise was found for balls with a diameter of 75 µm or 100 µm.

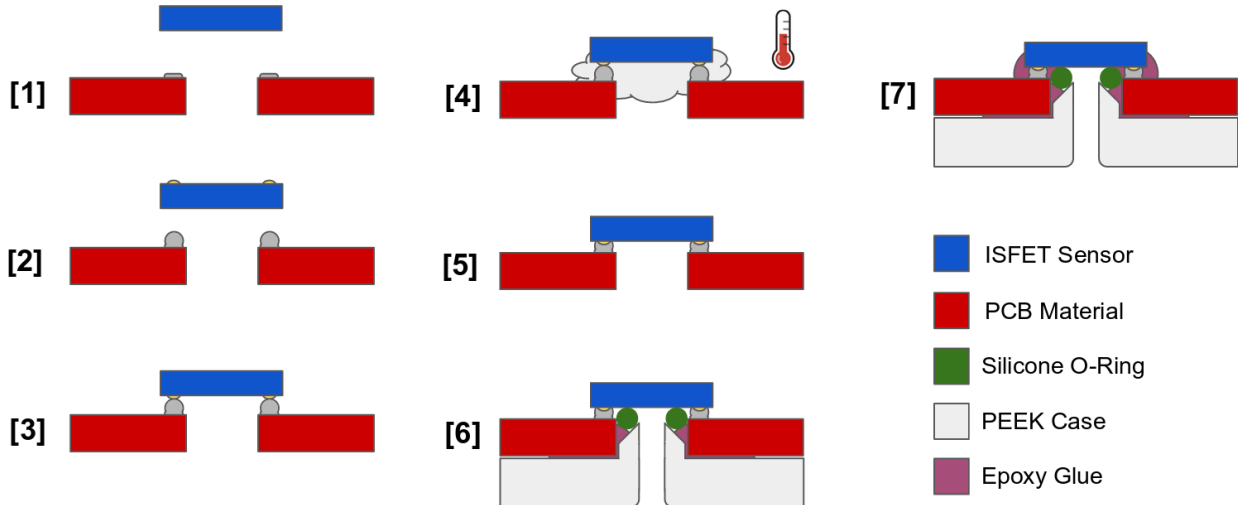


Figure 13: Overview of the sensor packaging process. Illustration created by author

The overall process can be explained with [Figure 13](#):

- [1] The wafer is diced into individual sensor dies. The PCB is finished with HASL (hot air solder leveling) by the manufacturer.
- [2] Studbumps are applied to the dies bondpads using an (automatic) wirebonder. The PCB is prepared by applying solder paste or solder balls onto the solder pads using a stainless stencil.
- [3] The ISFET die is placed and aligned onto the PCB by using a pick and place machine or an alignment stencil. Alignment can be checked using xray inspection.
- [4] The PCB is heated to 280 °C for 10 seconds using a hotplate. Additional flux is applied to ensure proper wetting of the platinum surface.
- [5] The ISFET is soldered onto the PCB.
- [6] The O-ring is placed inside the hole in the PCB under the ISFET. Then epoxy adhesive[\[18\]](#) is applied to the housing and the sensor board is placed on the gasket mandrel.
- [7] Additional glue is applied from the top of the sensor PCB as underfill of the flip chip sensor die. This adds mechanical strength and provides additional protection again moisture that might leak from the O-ring.

When SMD components are assembled, it is usually possible to cope with certain inaccuracies in positioning, as the surface tension of the melting soldering tin can easily correct misplaced components. However, since the ISFET sensor is very heavy in comparison to the very small solder balls, a very precise alignment is required before soldering.

Initially, this was ensured by X-ray inspection. The chip was optically placed in an approximately suitable position, X-rayed and then aligned until the bond pads visible in the X-ray align with the board structures.

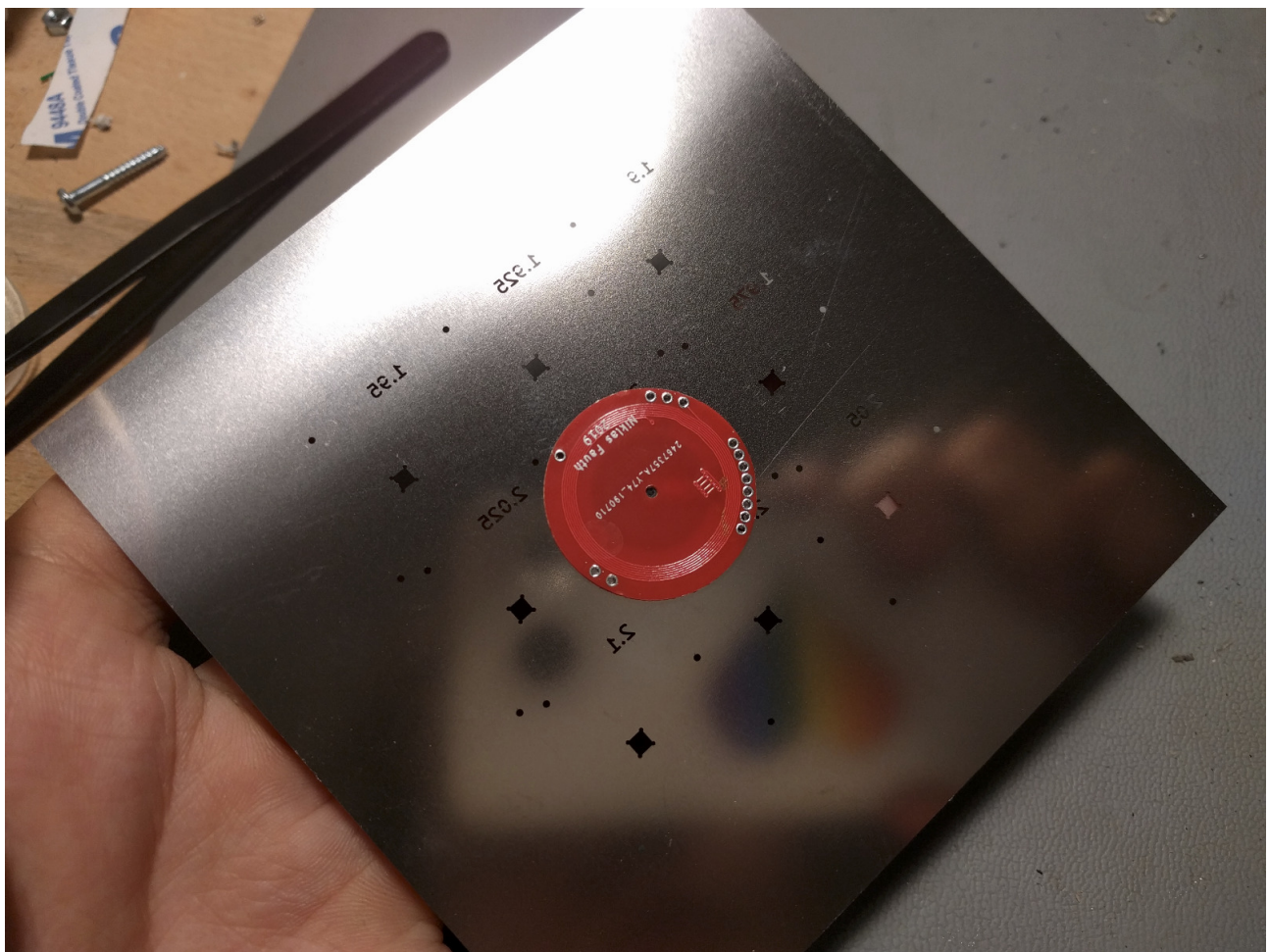


Figure 14: Stainless steel stencil with nine different alignment designs.  
Photo created by author.



Figure 15: Aligned stencil without the ISFET sensor.  
Photo created by author.



Figure 16: Sensor placed in stencil, ready for soldering.  
Photo created by author.

As this is time-consuming, a stainless steel stencil (Figure 14) was later redesigned, similar to the one used to apply the soldering paste from (Figure 13). Since the exact manufacturing tolerances were unknown, openings of different sizes were provided. The stencil can be placed on the board using fitting bolts. The ISFET sensor is then placed in the 2.025 mm rectangular hole. The stencil is heat-resistant and can remain during soldering. For mass production, this process can be further simplified by using modern pick-and-place machines.

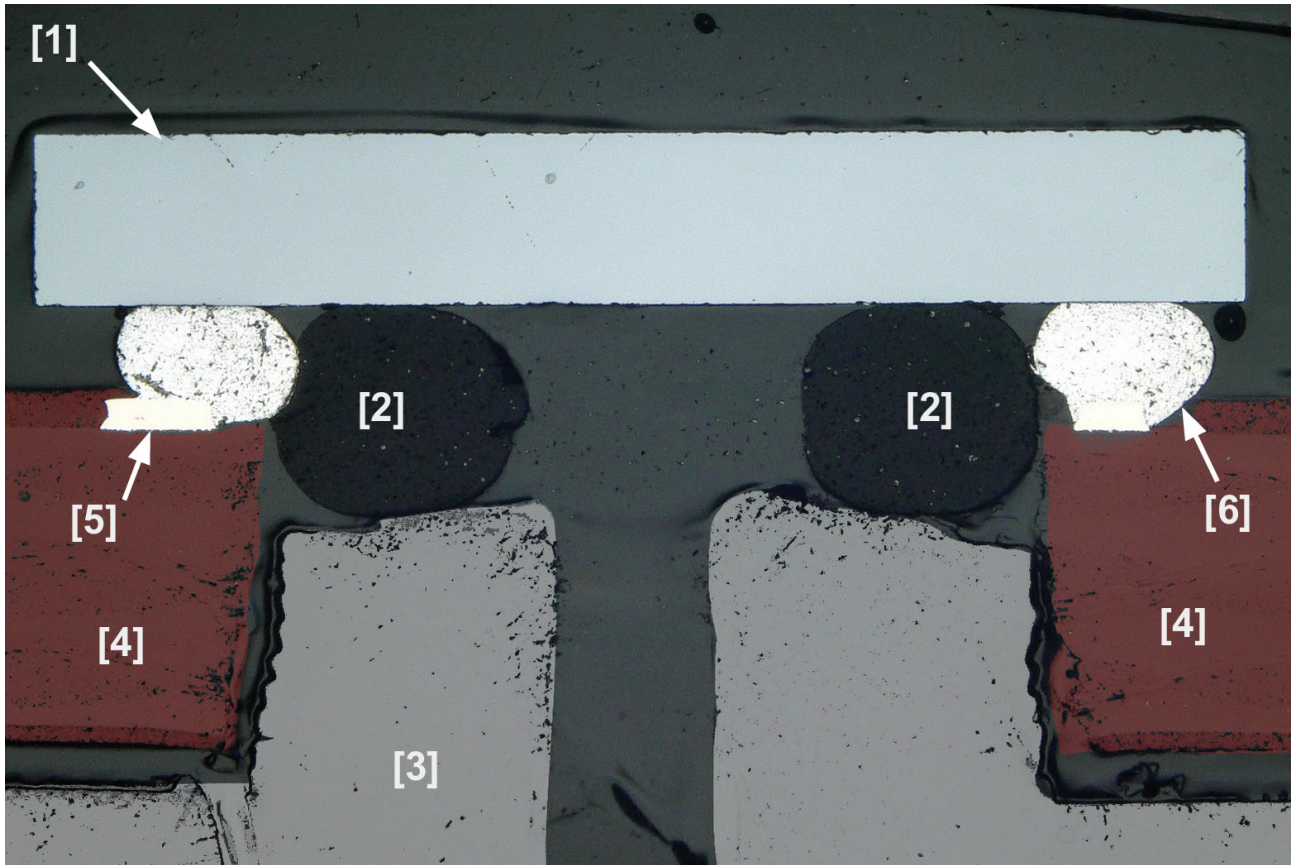


Figure 17: Colorized cross-section of the assembled implant.

Photo contributed by Texas Instruments.

- |                  |                        |
|------------------|------------------------|
| [1] ISFET die    | [4] Sensor PCB         |
| [2] O-ring       | [5] PCB trace (copper) |
| [3] Implant case | [6] Solder ball        |

#### 4.2.3 Future Improvements

For a future version of this ISFET sensor, it is already planned to overcome these issues by making increasing die size (3 mm x 3 mm instead of 2 mm x 2 mm) and by larger pad pitch to a standard pitch for chip scale packages. However, as this requires a new mask set, the start of production of this revision was not within the timeframe of this thesis.

Even though the current solution is much more complicated than hopefully will be the case with the future chip revision, the developed solution approaches could perhaps also be of interest to develop an even smaller implant. A long-term goal still is to make the ISFET sensor as small as possible, and being able to deal with the current size certainly is worth the effort.

## 5 Implant Electronics Design

### 5.1 System Overview

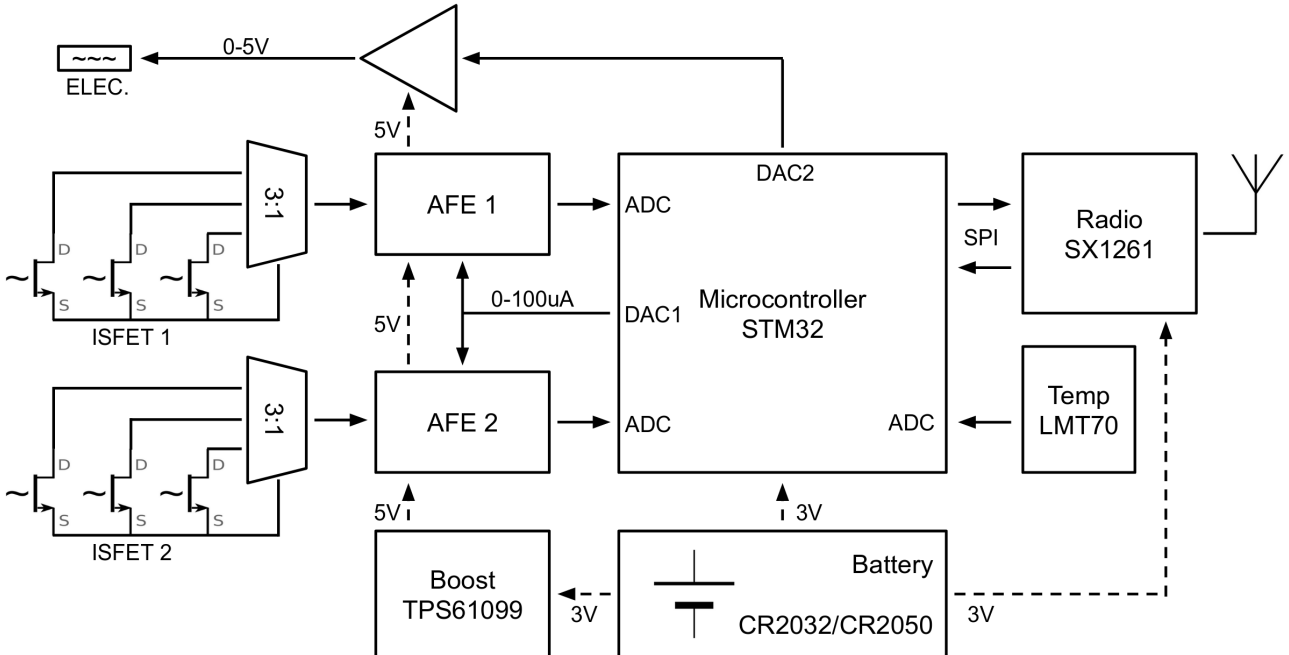


Figure 18: System Overview. Illustration created by author

Despite its small size, the implant contains a complex embedded system. The main CPU controlling the implants peripherals and reading sensor data from the ISFET AFE (Analog Front-End) is a STM32L072 ARM<sup>TM</sup>M0+ low power microcontroller. This MCU (Microcontroller Unit) was chosen for its rich both digital and analog peripherals, and for its low power architecture that allows switching off unneeded peripherals to save power. Also this MCU, despite the 33 electrical pins required, is very small in size as it is available in a "WLCSP-49" CSP (Wafer Level Chip Scale Package), measuring only 3.3 mm x 3.25 mm.

The STM32 communicates with a SX1261 LoRa radio transceiver IC via SPI (Serial Peripheral Interface). Apart from that, mostly analogue peripherals are used: Multiple ADCs (Analog-to-Digital Converter) digitize the ISFET sensor readings. Two DACs (Digital-to-Analog Converter) are used to adjust measurement parameters, one to set the ISFET drain-source current  $I_{DS}$  in a range of 0 to 100  $\mu$ A, and the other to adjust the gate electrode potential for both ISFETs. Precise temperature is measured with an integrated LMT70 analog temperature sensor, digitized by yet another ADC channel. In total, 11 ADC channels, 2 DAC channels, 1 SPI interface and 16 GPIOs (General-Purpose Input/Output) are used.

The AFEs contain the constant-current, constant-voltage sources necessary for stable operation of the ISFET sensor. One AFE contains readout circuitry for one ISFET + one corresponding REFFET. Multiplexers are used to attach the different ISFETs per die to the AFEs.

## 5.2 Battery and Power

The battery is the biggest single part in the implant and thus contributes most to the overall size. To select a suitable battery, the most important parameter hence is the power density by volume.

Battery comparison				
Cell chemistry	Common name	Rechargeable	Nominal voltage (V)	Energy density (Wh/L)
Zinc-air	PR	No	1.45–1.65	1673 [19]
Lithium-carbon monofluoride	BR	No	3	440–1478 [20]
Lithium-manganese dioxide	CR	No	3	300–710 [20]
Lithium-iron disulfide	FR	No	1.5	580 [21]
Lithium nickel manganese cobalt oxide	Li-Ion	Yes	3.6	580 [22]
Nickel-metal hydride	NiMH	Yes	1.2	401 [23]

According to this comparison, sorted from lower to highest power density, zinc-air batteries are by far the most suitable battery for this application. They are in fact widely used in the medical context, especially as button cells for external hearing aids. Unfortunately, they rely on oxygen in the air in order to operate, and are not usable for sealed applications like an implant. The second best power density is available with Lithium batteries. Both BR- and CR type batteries are commonly available in a button cell form factor (eg. the very popular CR2032 battery used for many consumer electronics remotes). A button cell is well suited for this application, as it is round and thin in shape, and is easy to use as it is already properly packaged (unlike most LiIon cells).

Common sizes are CR2032 / BR2032 with a diameter of 20 mm and a thickness of 3.2 mm, and CR2050 / BR2050 thickness of 5 mm. Typical capacities for these batteries are 210 mAh / 0.62 Wh (CR2032W [24]) resp. 345 mAh / 1.02 Wh (CR2050W [25]).

Power is supplied from the button cell straight to the STM32 and SX1261, with a voltage varying from 1.8 V to 3 V depending on the state of charge of the battery. For most of the electronics inside the implant this is not a problem as it operate with a voltage down to 1.65 V. The AFE however requires a higher voltage, as it needs to swing its output voltage over the full V<sub>th</sub> range of the ISFET, ranging from 1.0 V up to 1.5 V for higher pH values. Thus it is necessary to convert the battery voltage to a stable, higher voltage.

This is done by using a TPS61099 boost converter. This device is optimized for low power, battery powered applications. Especially the quiescent current of 800 nA and the internal power switch to disconnect the output in shutdown mode helps saving battery capacity as the AFE is unused most of the time. The TPS61099 is the fixed-voltage version of the TPS6109 with an output voltage of 5V. Other output voltages are available with an external voltage divider for the feedback input. For future sensors with lower V<sub>th</sub> this can be used to lower the AFE supply voltage and thus power consumption.

After assembly of the implant, a long period of time might pass before the implant is used for a study. As the battery is non-replaceable, it is necessary to assemble it during production. Even with the low sleep power consumption of the circuit, this would reduce battery lifetime.

To save power during storage, the implant implements a deep-sleep mode. A p-type MOSFET is used to disconnect the battery from the embedded system during storage. The implant can then be activated by an external alternating magnetic field. A coil on the lower sensor PCB, tuned to 13.56MHz, picks up the signal which is then being used to switch on the MOSFET intercepting power. Once the implant is powered and booted, a GPIO of the STM32 is pulled high to latch the MOSFET. LoRa communication can then be used to advise the STM32 to pull the pin low again, entering deep-sleep. This feature can be used for factory testing or if the implant was activated by accident.

13.56MHz is a popular ISM band for NFC (near-field communication). As no communication is required, a static field such as transmitted by a NFC reader or induction coil is sufficient to wake up the implant before surgery.

### 5.3 Multi-PCB Integration

For the assembled implant, all the electronics cannot simply be placed on a single PCB like one might do for a prototype or mechanically less complex device. For the Implant to work as required, and to be as small as possible, a rather sophisticated 3D design that holds all components in place and connects all electrical signals.

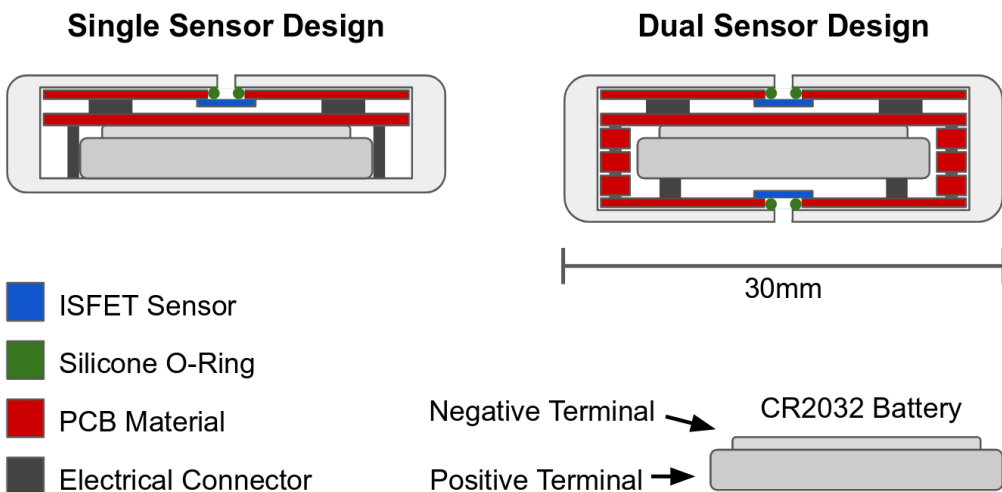


Figure 19: Comparison of internal structure for single sensor and dual sensor implant. Illustration created by author

As of the flipchip-design used for mounting the ISFET die, it is favourable to mount the ISFET sensor on its own, designated circuit board. This makes these sensor PCBs easy to manufacture as there is only a single device mounted on them (except for the electrical connectors). Also, in case of a defect, the PCB can be replaced without wasting additional components, saving cost during development and in cases of low successful soldering yield of the flip-chip ISFET. All other electronics is located on the mainboard, which is densely populated and can be produced by reliable, industry standard third party assembly services.

Because of this design decision, even a simplified, theoretical single sensor implant design requires an electrical connection between the upper sensor board and the mainboard. 10-Pin SMD (Surface-mount technology) mezzanine connectors [26] made by Hirose have been used for this as they are reliable and inexpensive. Also, they provide a spacing of 1 mm between the sensor- and mainboard, creating enough space for all the components on the mainboard, and the ISFET die on the sensor board.

For the dual sensor implant design, connecting component becomes more complex. The biggest issue is routing connections around the battery: Both ISFET sensors have to be connected to the mainboard, but with the battery in the middle of the implant, there is a massive obstacle in between the mainboard and the lower sensor.

With a distance of 3.2 mm to be bridged on a narrow edge of only 2.5 mm, there are no suitable SMD connectors. One possibility would have been to use wires soldered to both the mainboard and the sensor board, going around the battery. A more elegant and less labour-intensive way was found using stacked PCB rings that can be stacked by reflow soldering up to the required height. Rings have been ordered with 1mm and 1.6 mm PCB thickness. The PCBs have no components assembled and simply have pads on opposite sites, connected by vias. The rings are prepared with solder paste which is applied using a stencil. Before reflowing the mainboard, the rings are stacked to the desired height (eg. two 1.6 mm and one 1 mm ring for a CR2032 battery) and the mainbaord is placed on top, to form a single connected component during soldering. Once the battery is placed in the created pocket, the power sensor board is placed under the lowest ring and soldered to the ring's pads through the solder holes on the edge of the sensor board PCB, visible in [Figure 14](#).



Figure 20: PCB rings used for connecting the lower ISFET sensor.  
Photo created by author.



Figure 21: Exploded view of electronics. Photo created by author.

## 5.4 Communication

Due to the long distance through the tissue, magnetic-based near field technologies operating at around 10 MHz require too big coils as it would be practical for an implant. The required small size calls for higher frequency in order to get away with smaller antennas. 2.4 GHz, for example, is a popular high-frequency ISM (Industrial, Scientific and Medical) band used for WiFi and bluetooth. The problem with this is that absorption of electromagnetic waves by water increases with frequency, especially above 1GHz. Also, semiconductor-based transceivers get less efficient at higher frequency, reducing the battery lifetime additionally.

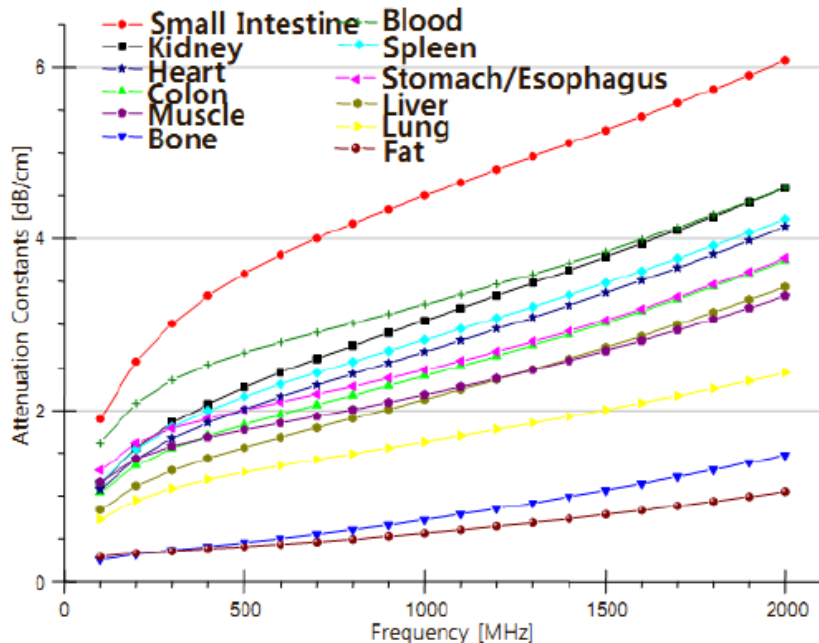


Figure 22: The attenuation constants for various parts of the human body. Illustration taken from "Communication Strategies for Various Types of Swallowable Telemetry Capsules" [27]

The existing Medical Implant Communication Service (MICS), used eg. for parametrize pacemakers, thus uses frequency band of 401 to 406 MHz. Unfortunately, only very few transceiver ICs exist that comply with the MICS standard. The only currently commercially available solution is the ZL70323 transceiver module from Microsemi [28]. Usage of this band requires special certification.

A compromise was found at a frequency of 868 MHz. This is a license-free short-range device (SRD) band in Europe and can be used without many limitations. Small, efficient antennas can be build at this frequency and absorption is acceptable.

### 5.4.1 Antenna Design

In order to achieve the longest possible range even with low transmission power, a high antenna efficiency is required in addition to a sensitive receiver. Since the implant moves spontaneously in relation to the base station, for example in animal experiments, a strong directional effect is undesirable. Having some directional gain towards the surface of the body is favorable through, as power that is transmitted towards the center of the body is mostly absorbed anyway.

Since 868 MHz is an industry standard frequency band, there is already a wide selection of ready-made antenna modules and designs.

For example, Linx offers the uSP Series microSplash™[\[29\]](#) embedded antenna modules that can be soldered to a circuit board. However, since these modules have been calculated for use in air, they require clearance to neighboring components and copper surfaces that cannot be realized in the implant.

A solution that is more easy to integrate into this tight design is a PCB antenna. PCB antennas are flat copper structures on standard PCB material that are designed in a way to form a antenna with certain specs.

There is a variety of different PCB designs and concepts for all kinds of applications. Silicon Labs published an application note of various PCB antenna designs including measurement reports [\[30\]](#), all designed for a frequency of 868 MHz. This was used as inspiration for a possible PCB antenna design.

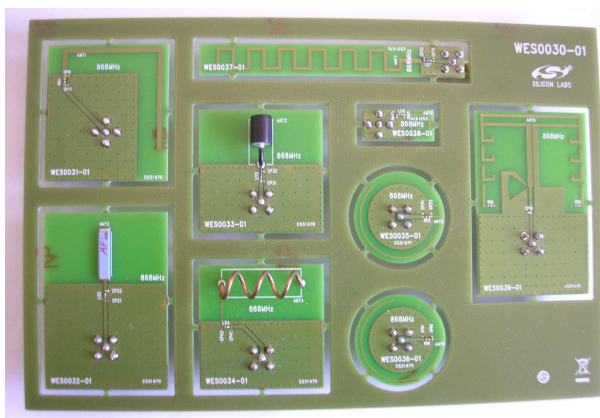


Figure 23: Different (PCB) antenna designs evaluated by Silicon Labs. Image taken from "SiLabs AN782: 868-MHz Antenna Matrix Measurement Reports"[\[30\]](#)

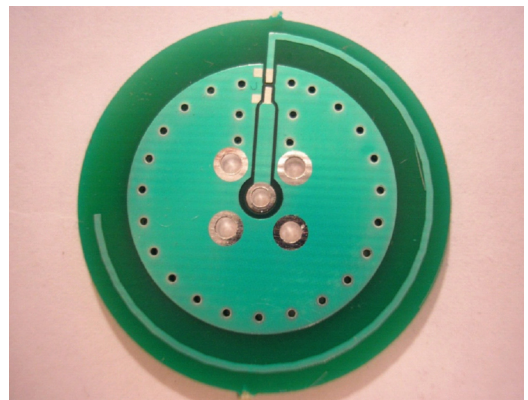


Figure 24: Silicon Labs Panic Button ILA (Inverted L Antenna). Image taken from "SiLabs AN782: 868-MHz Antenna Matrix Measurement Reports"[\[30\]](#)

One design that seemed to be best suited for the implant is the "Inverted L" antenna design which is advertised by silicon labs for use in panic buttons. Due to its round shape, it can be easily integrated into the implant.

The original design requires an outer diameter of 35 mm for the PCB which would be too big for the implant. However, since this was calculated for 868 MHz in air and the dielectric constant for the PEEK housing, surrounded by tissue, is higher than for air, the antenna as calculated for the implant may be smaller and therefore suitable.

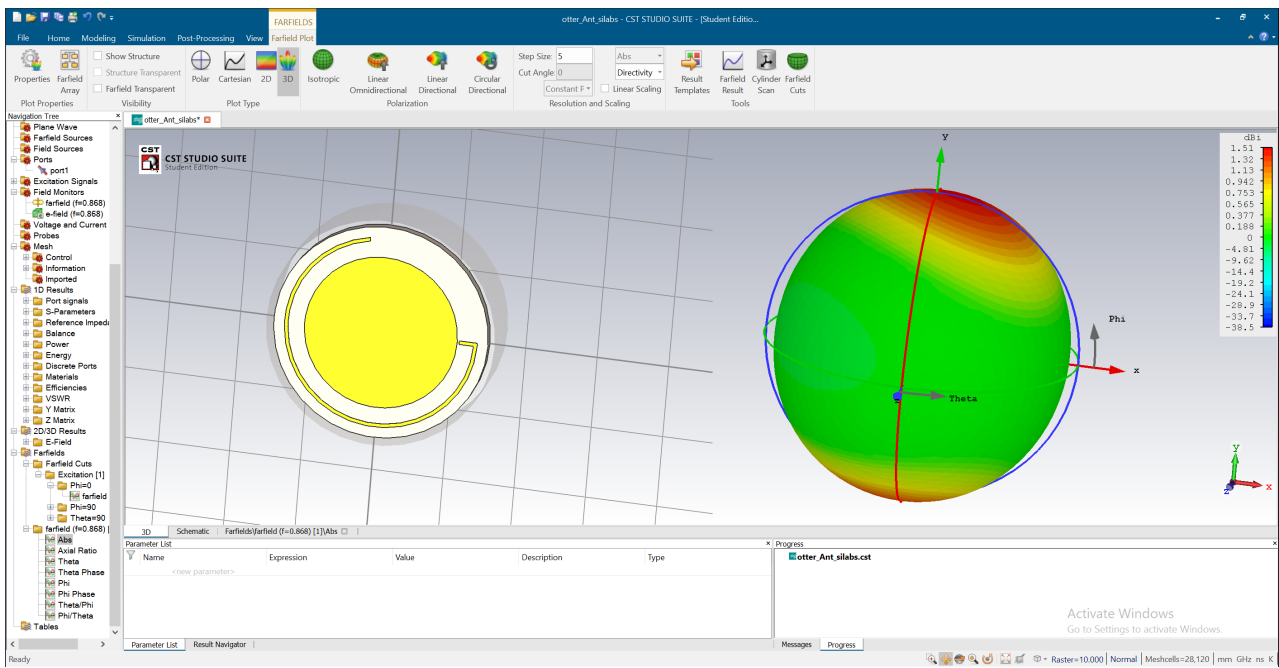


Figure 25: 3D model and Farfield Analysis of the PCB antenna assembly in CST Studio

To find the right dimensions to tune the PCB antenna to 868 MHz given the PEEK and tissue surrounding, CST Studio was used to simulate the antenna. For this, a simplified 3D model representing the PCB, PEEK case and surrounding tissue was modelled. Using automatic parameter sweeping, the antenna's arc length, ground clearance and trace thickness was optimized for maximal efficiency at 868 MHz with a feedline impedance of 50 Ohms. This is done by optimizing the VSWR (Voltage Standing Wave Ratio) for a value close to 1.0:1, as this simplifies the required matching network. CST Studio was then used to calculate the complex impedance of the antenna to get a starting point for calculating the matching network component values required for the LoRa transceiver.

The final design has a simulated VSWR of 2.1:1 for a 50 Ohm feedline. With 9dB return loss this can be considered an acceptable antenna given the high requirements in size. With a simulated complex impedance of  $32 + j 4.5$  Ohm a small Pi matching network can be used to match the LoRa transceiver's 50 Ohm output to further increase efficiency.

The expected radiation pattern was simulated using CST Studio as well. The antenna is placed on top of the implant, so the RF-blocking electronics and battery is faced towards the tumor, and thus towards the center of the body. The antenna shows a uniform radiation pattern, with a maximum gain of just 1.5 dBi.

The dimensions from CST Studio were then used to design the upper sensor PCB. As the transmitter is located on the mainboard, a connector was required to bring the feedline signal from the mainboard to the antenna. As proper RF connectors suitable for this application are too big in size to fit onto the heavily populated mainboard, unused pins of the already existing SMD mezzanine connectors [26] are used. This is not ideal as they are not impedance-matched and thus may reflect some of the signal, but given the small distance to bridge of just 1 mm this was considered irrelevant. The surrounding pins of the connector are used for good ground return to at least ensure some signal integrity.

After the first PCBs have arrived, SMD connectors were soldered to the antenna and mainboard PCB. A thin coaxial cable was soldered at one of the pads designated for the matching network.

## 5 IMPLANT ELECTRONICS DESIGN

The PCBs were then glued into a implant case prototype and a dummy battery was attached.

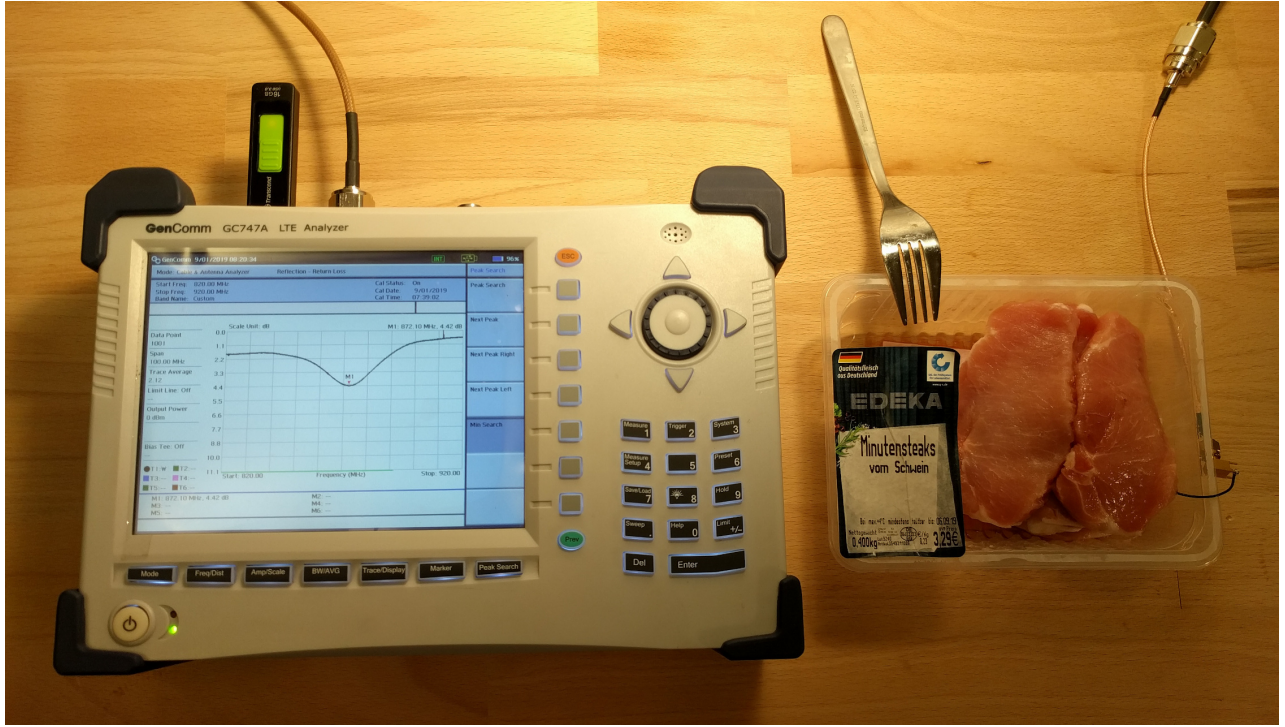


Figure 26: Measuring antenna parameters in an assembled implant buried in pork. Photo created by author.

A GenComm GC747A VNA (Vector Network Analyzer) was used to measure the actual impedance of the antenna. Since the environment of the implant has an influence on the antenna parameters, pork meat was used to simulate the effects within the body. Small changes to the PCB design were made in the course of other changes regarding the sensor footprint to further optimize the antenna for maximum efficiency.

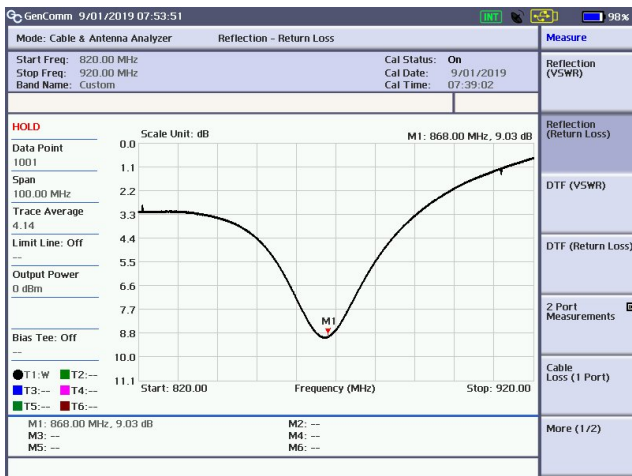


Figure 27: Return loss of the unmatched PCB antenna. Photo created by author.



Figure 28: Smith chart of the unmatched PCB antenna. Photo created by author.

The packaged antenna impedance was measured to be  $24 + j 1.4 \text{ Ohm}$ . Since the transceiver

IC calls for a 50 Ohm matched antenna, a PI matching network can be used to maximize power transfer from transceiver to antenna and thus minimize power consumption.

### 5.4.2 Transceiver Selection

For the 868 MHz frequency band, multiple transceiver ICs are available. They mainly differ by the modulation techniques and protocols they support. The following ICs have been considered for this application:

- Texas Instruments CC1312R [31]
- HopeHF RFM69CW [32]
- Semtech SX1261 [33]

All of these ICs are state of the art transceivers capable of operation over a wide frequency range, including the 868 MHz license-free SRD860 band [34]. Nevertheless there are differences which are more or less suitable for this application. For example, the CC1312R includes a cortex M4F CPU which is fully programmable. This would have allowed to use the CR1312R standalone as both integrated radio and microcontroller, reducing parts count and system complexity compared to a discrete solution. The RFM96CW does require an external microcontroller, but has all the RF matching components included, also reducing parts count.

Still, the SX1261 has been chosen for this project. This IC requires both an external microcontroller and additional RF matching components. However, the SX1261 supports a modulation technique not available for the other two candidates: LoRa (Long Range) and LoRaWAN (long range wide-area network).

One of the requirements for the implant was compatibility and long-term software support. Server-side software for data acquisition and processing, characterization, long-term lifetime test and actual experiments on animals using the implant are not within the scope of the thesis and will be performed by people from different fields of research. Since the radio is the interface between the development covered in this thesis and future research involving the implant, a custom solution should be avoided.

While most modulation techniques are standardized, using either the RFM69CW, CC1312R, or most other sub-1GHz transceiver ICs would require developing not only the transmitter in the implant but also some sort of base station. Only very few commercial radio ICs below 2.4GHz support standardized protocols, and even fewer of these protocols are suitable for this application where low data rate, but low-power and high resilience against interference.

LoRa is a spread spectrum modulation technique, the first commercial implementation of chirp spread spectrum for low-cost applications [35]. Using Forward Error Correction coding and an extremely high wireless link budgets (up to 170 dB)[36], LoRa enables long-range transmissions (more than 10 km) and is mostly used for Internet of Things (IoT) applications. However, these properties can also be off favor for applications like an internal implant, where distance is low, but damping is high due to absorption in the body.

Both LoRa, the physical layer of LoRaWAN, and LoRaWAN, the protocol for upper layers of the network, are maintained by the LoRa Alliance. Multiple IC manufacturers are part of this Alliance to ensure interoperability of all LoRaWAN devices and radio ICs.

Because of the wide usage of LoRaWAN for all kinds of IoT applications, lots of LoRaWAN to TCP/IP (either via Ethernet or WiFi) gateways are available off the shelf. These gateways

are required for receiving the packets from the implant and sending measurement data to a server for storage and processing. Thanks to the LoRa Alliance, products from a variety of manufacturers are compatible, offering different features like IP67 rated gateways for outdoor use, which is relevant for applications involving livestock.



Figure 29: Laird Sentrius™ Indoor Gateway. Photo created by author.

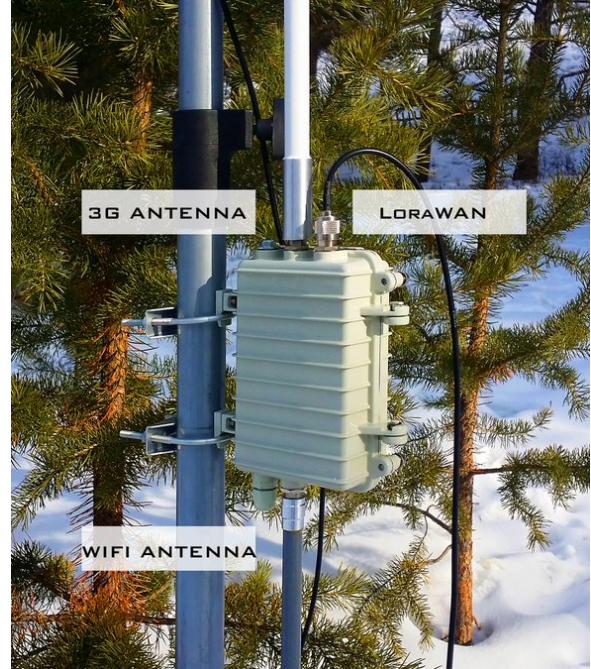


Figure 30: Outdoor LoRaWAN Gateway for remote applications.<sup>3</sup>

One more advantage of LoRaWAN is the big community that has formed around this technology. There are many open source software projects available that are useful for setting up applications using LoRaWAN (like LoRa Server[38]), and debugging is easy thanks to online resources. There even already exist online services that can be used as a data endpoint for LoRaWAN packages, like TTN ([thethingsnetwork.org](http://thethingsnetwork.org)).

In conclusion, LoRaWAN rewards with less dependencies since using the implants does not require any custom additional hardware, compatible gateways can be bought off the shelf. Developing application software is easy as the protocol is standardized and many examples and services are available online ready to use.

---

<sup>3</sup>D.Batulzii,  
<http://www.sanchirtech.com/>

### 5.4.3 Transceiver Design

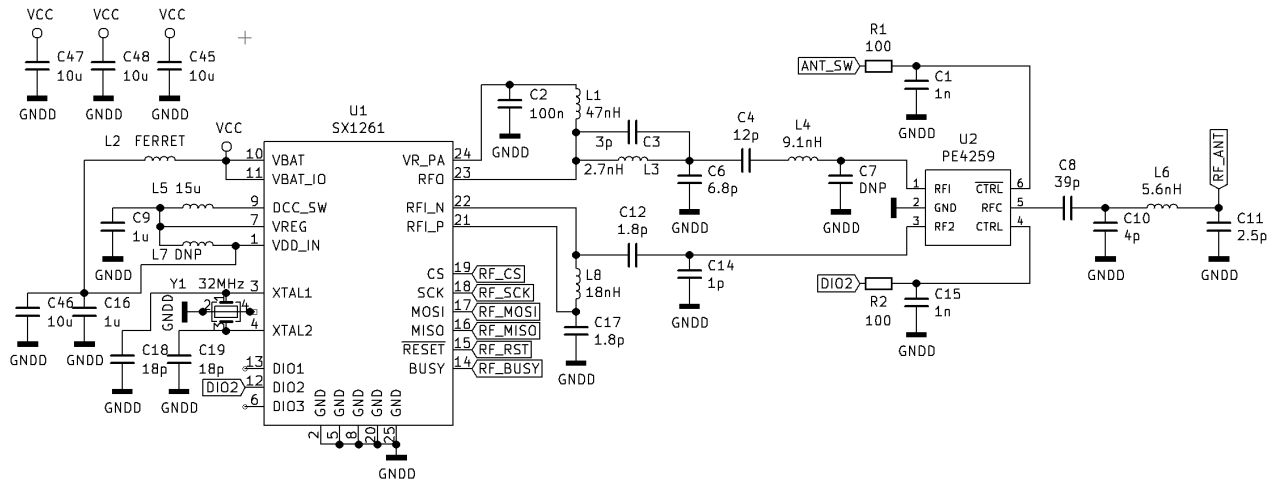


Figure 31: Section of the implants schematic shows the LoRa transceiver circuit.

The majority of the circuitry around the SX1261 has been adopted unchanged from the reference design[39]. Since the SX1261 has no internal receive / transmit switch, U2 is used to switch the antenna to receive (RX) or transmit (TX) mode. The components between the transceiver (U1) and the RF switch (U2) are used for filtering and impedance matching so that both the RX and TX line on pin 1 and 3 of the switch have an impedance of 50 Ohms. This also applies to the output (pin 5) of the RF switch. The values for these components can also be copied from the reference design, as long as the board layout takes care to use the same values for the width and clearance of the tracks, so that the stripline impedance is equal to the reference design.

To the right of the RF switch, a DC blocking capacitor and a PI network for antenna impedance matching to 50 Ohms is used to connect the antenna.

### 5.4.4 Antenna Matching

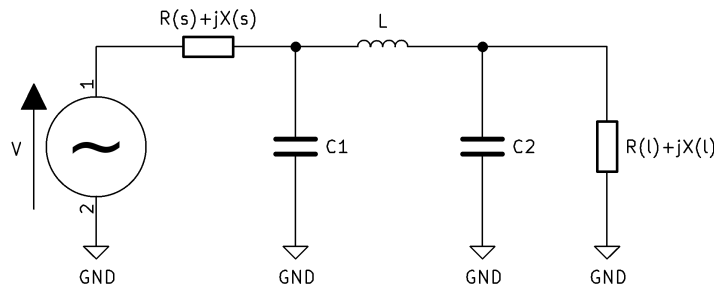


Figure 32: Circuit of a PI matching network. Illustration created by author.

This circuit is required to transform the antennas input impedance of  $24 + j 1.4$  Ohm to the 50 Ohm output impedance of the LoRa transceiver. There are also other circuits like a L matching network that can fulfill the same purpose. However PI networks are known to have better characteristics for matching high impedance sources to low impedance loads [40]

The component values can be calculated from the source impedance  $R(s) + jX(s)$ , the load impedance  $R(l) + jX(l)$ , as well as the quality factor, and the center frequency  $f$  to convert the reactances resulting from the following formulars to a component value.

The quality factor is usually defined as  $Q = f / \text{BW}$ , where BW is the bandwidth that can pass through the PI filter with less than 3 dB attenuation. It thus is a measure for harmonic attenuation of these networks. Since not much additional filtering is necessary at this point in the overall RF circuit, a quality factor close to 1 is desirable. Due to the higher bandwidth associated with a low Q factor, component tolerances are also of less importance.

The reactance required for  $C_1$  can be calculated as follows[41]:

$$X_{C1} = -R_S \left[ \frac{2QR_S + \sqrt{4Q^2R_SR_L - (R_S - R_L)^2}}{R_S(4Q^2 + 1) - R_L} \right] \quad (5.1)$$

Choosing  $Q = 1.1$ , this results in  $X_{C1} = 45.5$  Ohms. For 868 Mhz, 4pF are required.

$$X_{C2} = -R_L \sqrt{\frac{R_S X_{C1}^2}{R_L R_S^2 + (R_L - R_S) X_{C1}^2}} \quad (5.2)$$

Using the result from Equation 5.2 this results in  $X_{C2} = 77$  Ohms. A value of  $C_2 = 2.5$  pF is chosen.

$$X_L = -(X'_{C1} + X'_{C2}) = -X_{C1} \frac{R_S^2}{R_S^2 + X_{C1}^2} - X_{C2} \frac{R_L^2}{R_L^2 + X_{C2}^2} \quad (5.3)$$

Last, the required inductance can be calculated. A inductive reactance of 30.65 Ohms is required, which can be achieved by using a 5.6 nH inductor.

## 5.5 Sensor Readout Circuit

This circuit part is responsible for operating the ISFET sensor at a suitable operating point, so that the determined thresholds voltage can be measured by the ADC of the microcontroller.

### 5.5.1 Analog Front-End

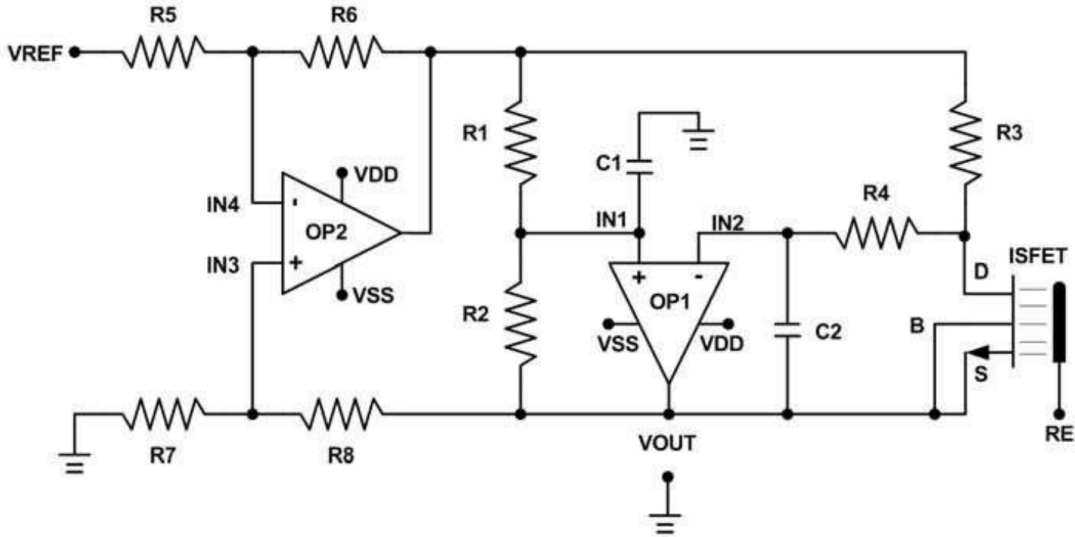


Figure 33: Traditional ISFET bridge-type readout circuit. Figure taken from "CMOS Readout Circuit Developments for Ion Sensitive Field Effect Transistor Based Sensor Applications" [42]

This circuit is commonly used for ISFET test setups, as it offers a simple and stable method of operating the ISFET in CCCV mode. The operational amplifier OP2 is used to create a floating reference voltage between its output and the source of the ISFET, with equal potential as VREF to ground in case  $R_5 = R_6 = R_7 = R_8$ . OP1 is used to ensure a constant current flowing through the ISFET. As the voltage potential between IN1 and IN2 of OP1 is supposed to be 0 V, the voltage drop over  $R_1$  is equal to the drop over  $R_3$ , and thus the voltage drop over  $R_2$  is equal to the ISFETs  $U_{DS}$ . Therefore, the drain-source voltage and current of the ISFET can be calculated as follows:

$$V_{DS} = V_{R2} = V_{REF} \left[ \frac{R_2}{R_1 + R_2} \right] \quad (5.4)$$

$$I_{DS} = I_{R3} = \frac{V_{REF} - V_{DS}}{R_3} \quad (5.5)$$

This circuit uses a gate electrode referenced to ground, which simplifies the test setup in most cases. Same as with MOSFET, p-channel and n-channel type ISFET can be constructed. Since n-type ISFETs were provided by Texas Instruments, a negative voltage rail is required for VSS as  $U_{GS}$  is positive for n-type fets, but with  $U_G = 0$  V, source would have to swing negative. This becomes a problem for embedded applications such as the implant, as negative voltage rails introduce additional complexity for both the power management and the signal conditioning (the ADC of most microcontrollers can only accept positive voltages).

The circuit can be modified to work with solely positive voltages by referencing the gate voltage to a positive rail, eg. the VDD supply voltage of the opamps, or an adjustable  $U_{\text{electrode}}$ . To change the sign of the floating voltage source, the VREF voltage has to be applied to R7, with R5 being the new ground reference.

This way the output voltage of the circuit,  $V_{\text{OUT}}$ , is equal to  $U_{\text{electrode}} - U_{\text{GS}}$ . Since the pH-dependent gate-source threshold voltage is proportional to  $U_{\text{GS}}$  for CCCV operation, the output voltage also becomes proportional with the pH concentration of the electrolyte.

Further existing optimization of this circuit, such as the two low-pass filter (LPF) formed by C1 and C2 can also be adapted to this slightly changed variation. This LPF helps increasing signal quality by filtering out external interference (p. 425 [42]) caused eg. by electromagnetic fields emitted by the LoRa transceiver or the boost converter. The passband edge frequency is calculated with

$$f_P = \frac{1}{2\pi (R_4 + R_3||R_{DS}) C_2} = \frac{1}{2\pi (R_1||R_2) C_1} \quad (5.6)$$

Since the analog bandwidth of the sensor subsystem is much lower than the high frequency interference, the exact cutoff frequency is not critical. Given the values in Figure 34, a  $f_P$  of 4.1 kHz provides sufficient interference suppression.

To compensate for drift effects and temperature dependency of the ISFET, the pH-independent  $U_{\text{GS}}$  of the REFFET has to be measured at a similar point of operation as the ISFET. This could be done by using an additional MUX to connect the AFE alternately to either the ISFET or the REFFET. However this would limit the sample speed as the ISFET needs to stabilize first for some milliseconds before taking accurate readings. Although the sampling time is not critical compared to the slow biological processes, a fast settling time is desirable to minimize the period in which the AFE is powered.

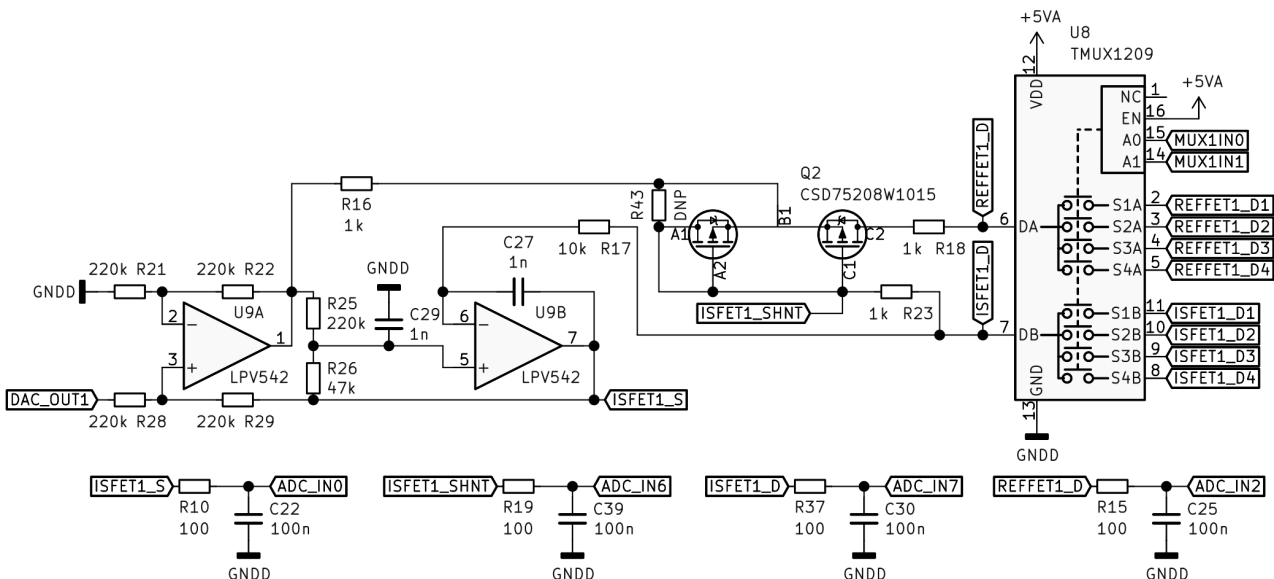


Figure 34: Section of the implants schematic shows one of the two AFE + MUX

(p. 437 [42], Fig. 20) thus suggests to extend the circuit with a current mirror. In Figure 34 this is implemented by Q2, using a CSD75208W1015 dual common source P ch MOSFET. This

current mirror splits the constant current through R16, allowing to operate both the ISFET and REFFET with equal drain-source current.

Being able to change the operating point in software can be favourable since the four different ISFET designs per chip might behave different, or to operate for some measurements at lower drain-source currents to save power. This can be achieved by connection one of the internal DACs of the STM32 microcontroller to the VREF input of the circuit. Since the STM32 uses an analog reference voltage of 2 V, the drain-source voltage of the ISFET can be adjusted over a range of 0 to 0.35 V. With the additional resistance introduced by the current mirror, the ISFET's drain-source current can be set to 0 to 320  $\mu$ A. A suitable operating point for the ISFETs used for this implant was found at  $U_{DS} = 0.25$  V,  $I_{DS} = 100$   $\mu$ A.

The TMUX1209 2-ch, 4:1 analog multiplexer (MUX) is used to connect the same AFE to one of the three ISFETs and corresponding REFFETs. Changing the selected ISFET is necessary in case of an early fault of one of the ISFETs, and check plausibility of results by comparison between sensors within the chip. The MUX is configured by the microcontroller using GPIOs. While the mainbaord is prepared to connect to all four ISFETs per die, due to the limited space and challenging sensor packaging, only three ISFETs are broken out on the sensor PCBs.

Additional reliability of the measured values can be achieved by in-system diagnosis of the AFE. In order to determine whether one of the sensors has failed due to aging or leakage, the drain-source voltage and current of the ISFETs can be measured in addition to the pure output voltage of the circuit. For this R23 is used as a current shunt, with an ADC channel attached on both terminals. For proper high-precision current sensing, this small voltage drop of 0.1 V per 100  $\mu$ A would be amplified using additional analog circuitry. This has been avoided since space is limited and this is only used for basic diagnosis. With ADC resolution of 12 bit this results in a current resolution of 0.5  $\mu$ A / least significant bit (LSB). Calculating the difference between ADC readings from ISFET drain and source,  $U_{DS}$  can be measured with a resolution of 0.5 mV / LSB.

To get best ADC accuracy, an external capacitor is necessary at each channel of the STM32 ADC. Since the ADC uses an internal sample-and-hold circuit, this capacitor is used to lower the source impedance of the channel as seen by the ADC so that the internal sample capacitor can be charged from the external capacitor quickly and without much load to the source. This is crucial for both the AFE circuit as well as the electrode sensing since both have very high impedance and would suffer distortion by sampling the ADC [43].

The external capacitor must have to store enough charge so that the voltage drops by less than 1/2 LSB when transferring charge to the sampling capacitor, since a bigger drop would affect the LSB of the ADC reading and thus limit resolution.

$$C_{ext} = 2^{12+1} \cdot C_{samp} \quad (5.7)$$

For a sampling capacitor with 8 pF, the minimum required external capacitor can be calculated to be 66 nF. This was rounded up to 100 nF, since this value is already used for decoupling.

The series resistor of 100 Ohm was added to form a low-pass filter with a cutoff frequency of 16 kHz, rejecting interference from the boost converter or radio. It also limits the maximum current flowing into the GPIO where a voltage larger the supply voltage of the STM32 is applied in case of a fault of the 5 V - powered AFE.

The circuit shown in Figure 34 is included in the implant twice, once per ISFET chip mounted on the two sensor boards.

### 5.5.2 Electrode Subsystem

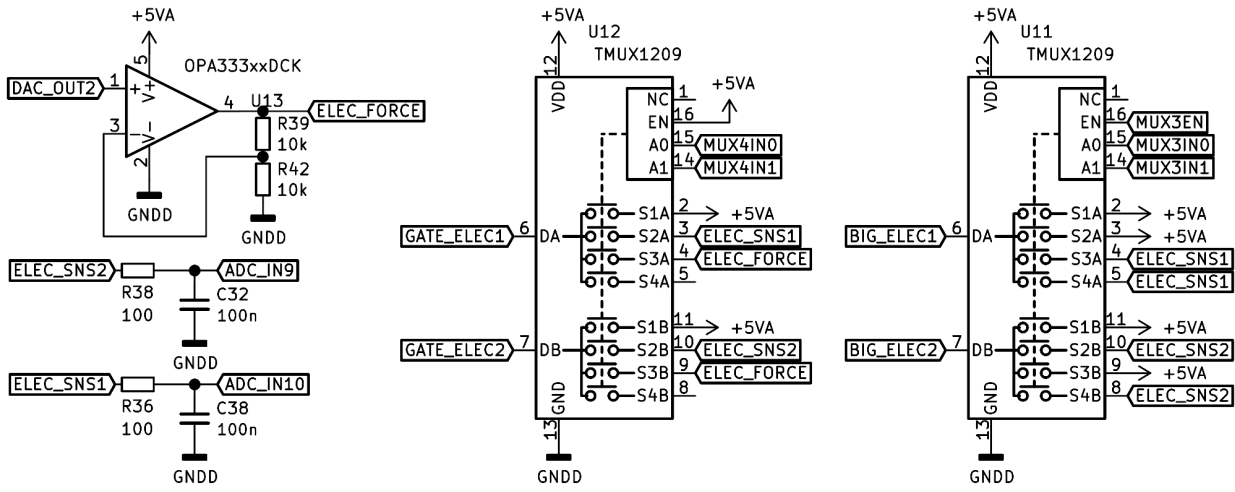


Figure 35: Section of the implants schematic shows the electrode control.

A total of four electrodes are available in the implant, one large electrode (BIG\_ELEC) and one gate electrode (GATE\_ELEC) for each sensor (1 / 2). In order to be flexible in the choice of measurements when inserting the implant, the wiring of the electrodes is correspondingly flexible and can also be changed in the body. In total there are four different ways an electrode can be connected using a MUX:

- No connection (NC). The MUX is disabled or switched to an unused pin. The electrode is floating.
- Electrode sense (ELEC\_SNS). The electrode is connected to an ADC input. Voltage can be measured in a range of 0 - 2 V with 40 kOhm impedance (corresponding to 0 - 50  $\mu$ A current to GND).
- 5 V constant voltage.
- Ground / 0 V with 100 Ohms impedance. This is done by setting the MUX to "sense", but configuring the GPIO of the STM32 not as ADC input, but as a GPIO output that is pulled low.
- Adjustable voltage 0 - 4 V (ELEC\_FORCE).

Among others, the following tests can be performed using the electrode connection matrix.

**For both sensors: Big Electrode = NC; Gate Electrode = Adjustable voltage:**

Normal pH measure operation. Since both sides of the implant have the same voltage applied to the gate electrodes, no current is flowing through the electrolyte. The ADCs for pH measurement are directly connected to the outputs of the AFE to get maximum resolution, with a ADC input range of 0 - 2 V. Thus care must be taken not to exceed the maximum input voltage. The highest output voltage of the AFE is the positive terminal of the  $I_{DS}$  current shunt. The voltage at this pin at a operation point of  $U_{DS} = 0.25$  V,  $I_{DS} = 100 \mu$ A is:

$$U_{SHNT} = 1k\text{Ohm} \cdot 100\mu\text{A} + 0.25V + (U_G - U_{G(th)}) \quad (5.8)$$

Where  $U_{G(th)}$  is the pH dependent gate threshold voltage of typically 1 - 1.5 V and  $U_G$  is the variable gate voltage applied to the gate electrodes in this mode. In this case, an electrode voltage of 2.5 V would result in an AFE output voltage of 1.35 V to 1.85 V which is safe to apply to the ADC input. Software on the STM32 is used to calculate safe reference voltage for different operating conditions. It would be possible to restrict the output voltage without software using a voltage divider on the ADC input, but this would decrease the effective ADC resolution and would cost additional parts and thus more space.

**For both sensors: Big Electrode = NC; Gate Electrode = Sense:**

This mode can be used to detect any defects of the ISFET sensors or the seal. Any current leaking through a broken gate substrate would cause a voltage to be measured at the ADC inputs. The ISFET MUX can be used to test all ISFETs.

**One sensor: Big Electrode = Adjustable voltage or 5V; Gate Electrode = Adjustable voltage or 5V. Opposite sensor: Big Electrode = Sense or GND; Gate Electrode = NC or GND:**

With the different voltage potential between the two sides of the implant, a current flow through the electrolyte / tissue is introduced that can be used to change the pH value around the sensor openings by electrolysis. This feature can be used to research how the tissue reacts to changes in pH concentration under treatment.

## 5.6 PCB Layout

In order to make it easy to replace the sensor boards for the purpose of design revision of the packaging, the mainboard was designed to combine as much electronics as possible on a single PCB.

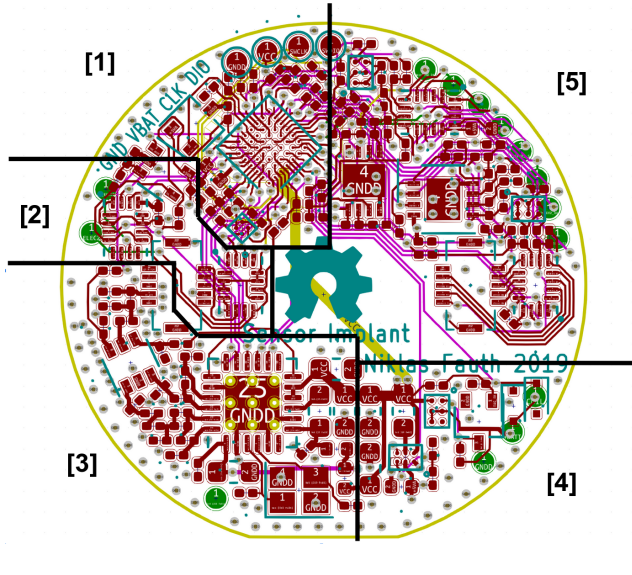


Figure 36: Screenshot of the mainboard PCB Layout. Copper pours are deactivated to show the inner traces.



Figure 37: Three assembled mainboards. Photo created by author.

The resulting circuit board (Figure 46) contains all the subsystems described before: [1] STM32 microcontroller with temperature sensor and voltage reference; [2] electrode subsystem; [3] RF transceiver with antenna matching; [4] power management; [5] analog front-end and sensor multiplexer.

The four-layer board with 0.8 mm thickness is mostly assembled with 0201 passives. Using modern ICs for all parts required by the circuit, a large selection of packages with small footprints was available and selected.

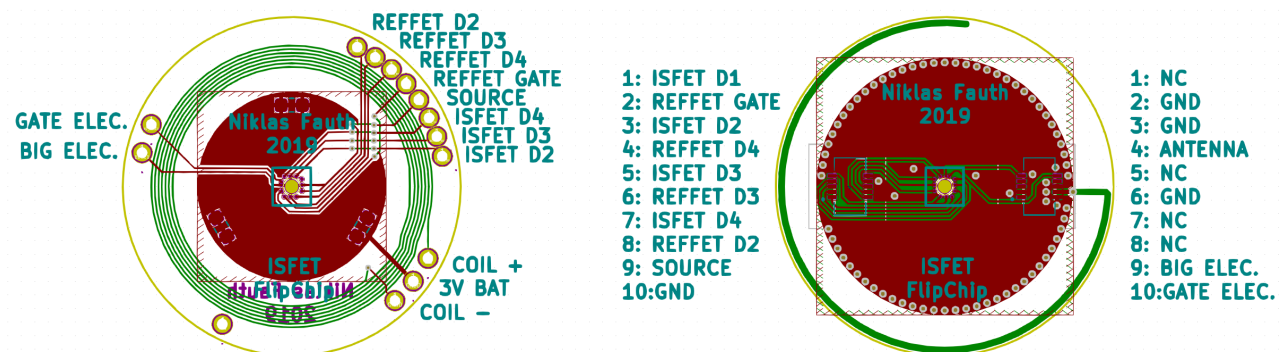


Figure 38: Screenshot of the sensor PCBs Layout.

The 0.6 mm thick sensor boards only contain the ISFET sensor, plus SMD connectors in case of the upper board. Additionally the upper sensor board integrates the PCB antenna for the

radio. A total of 7 windings on the bottom sensor PCB are used as the pickup coil to wake up the implant from deep-sleep.

## 6 Firmware and Software

### 6.1 Implant Firmware

The firmware running on the STM32 is written in C. The flashable binary can be compiled with GCC (GNU Compiler Collection) using a Makefile. Most peripheral initialization was generated by cubeMX, a code generation tool by ST Micro. The STM32 can be programmed and debuged via SWD (Serial Wire Debug). For this, four testpoints are exposed on the mainboards (GND, SWCLK, SWDIO and VCC) that can be contacted by soldering or, for mass production, spring-loaded contacts.

The software was mainly optimized for low power consumption. Therefore the ARM M0+ core, although it could run up to 32 MHz, is clocked most of the time with only 2 MHz. The power saving features of the STM32 10 series are also used in many places, so that e.g. peripherals like ADCs and timers are switched off when not used.

#### 6.1.1 Radio Initialisation

The SX1261 is connected to the STM32 via a SPI interface. With this interface, registers can be set and read so configure the chip, as well as to read and write the payload to be transmitted. In addition to this serial interface, three more GPIOs of the STM32 are connected to the radio, one for reset, "busy" to indicate the status of the internal state machine, and one for setting the RF switch to either transmit or receive.

The SX1261 can be configured for a variety of RF protocols. Communication with the gateway is done via LoRa. The following settings were selected to talk to the gateway:

RF_FREQUENCY	868.5 MHz
TX_OUTPUT_POWER	14 dBm
LORA_BANDWIDTH	125 kHz
LORA_SPREADING_FACTOR	SF7
LORA_CODINGRATE	4/5

Bandwidth is the frequency range of the chirp signal. For LoRa, three bandwidths are available to choose from: 125kHz, 250kHz and 500kHz.

The Spreading Factor (SF) defines how many chips are used to represent a symbol. The higher the SF value, the more chips are used per symbol, allowing the receiver to recover signals with lower signal-to-noise ratio.

The coding rate value (CR) defines how many bits are used for error correction. LoRa modulation uses forward error correction in every data transmission. This is done by encoding every 4 bit of data into 5 bit, 6 bit, 7 bit, or 8 bit by adding redundancy. Higher CR values means more resistance to interference.

The achievable data rate is defined by all these parameters. Typical data rates used for LoRa are [44]:

Data Rate	Configuration	bits/s	Max payload
DR0	SF12/125kHz	250	59
DR1	SF11/125kHz	440	59
DR2	SF10/125kHz	980	59
DR3	SF9/125kHz	1 760	123
DR4	SF8/125kHz	3 125	230
DR5	SF7/125kHz	5 470	230
DR6	SF7/250kHz	11 000	230

Using DR5, the radio was mostly optimized for high data rates and thus lower power since the given data is transmitted in shorter time. In case the maximum range has to be increased or interference cause problems with reliable data transmission, the data rate can be further reduced to eg. DR4.

### 6.1.2 Theory of Operation

After switching on the implant for the first time by applying the HF field to wake up from the deep sleep, the STM32 first sets GPIO PB14 to high in order to permanently latch on the battery switch. Then the SX1261 LoRa transceiver is initialized via SPI and a status packet is sent.

The implant then starts normal operation. To maximize battery life, most of the time the AFE and LoRa transceiver are switched off. The STM32 is in sleep mode and the CPU is switched off. Only a timer keeps running and wakes the controller up after a defined period of time.

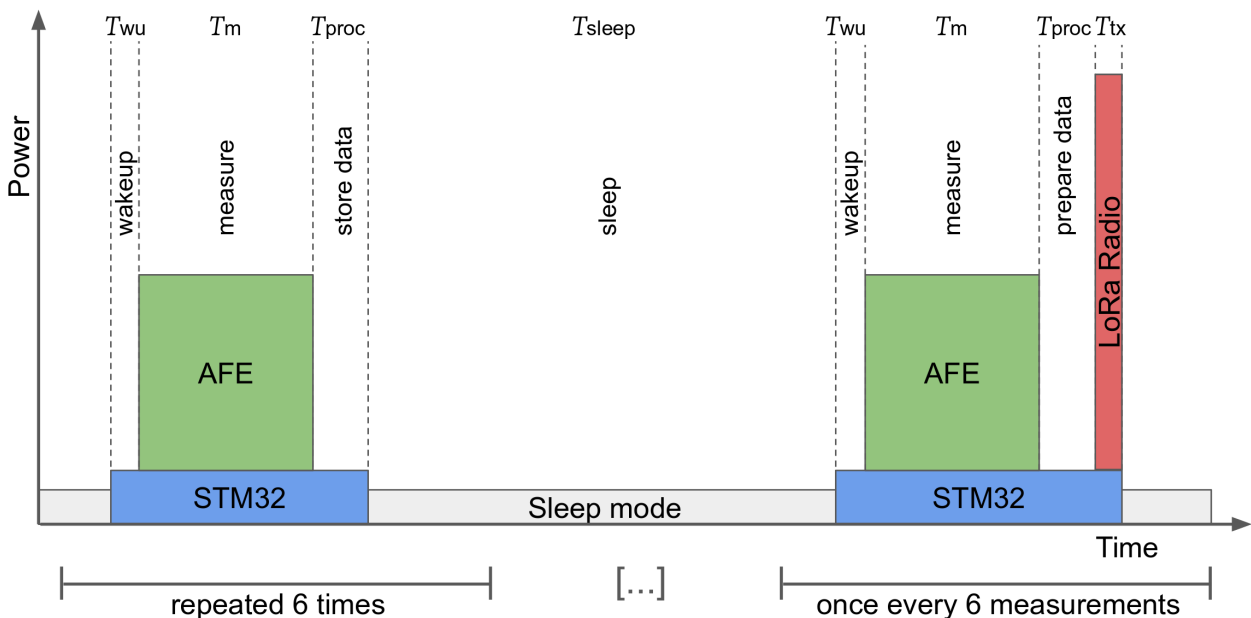


Figure 39: Time sequence of the implant functions. Illustration created by author

Once the STM32 started its CPU and initialized all peripherals required for measurement (ADC, DAC, GPIOs), the TPS61099 boost converter is powered on to supply the AFE. The STM32 then uses one DAC channel to set the ISFET operating point, and the other DAC channel to apply an electrode voltage. ADCs are sampled every 1 ms, multiple measurements are averaged for better accuracy. After some settling time, every ISFET on the sensor chip is

sampled and all gate threshold voltages are stored in flash, together with additional measurements like the AFE diagnosis values for each ISFET, as well as battery level and temperature. The full measurement takes  $T_m = 1$  s.

Most values are stored as 12 bits, the raw ADC resolution. One measurement contains up to 36 bytes. Since a maximum of 230 bytes can be sent per LoRa package, it is most efficient to send six stored measurements all at once every sixth measurement. Transmitting the payload takes  $T_{tx} = 22$  ms.

After transmitting, the LoRa transceiver switches to receive mode for a short amount of time. This timing window allows the gateway to respond to the transmitted measurements, eg. to change the measurement parameters or the sample rate. This has been tested successfully, however a proper protocol and end-user config tool is still to be implemented. All config currently is hardcoded in firmware and uploaded during programming the STM32.

## 6.2 Server-side Software

Working with the transmitted data of the implant is straightforward. For the purposes of this thesis, thethingsnetwork (ttn) was used for forwarding data to the users application. For most commercial LoRaWAN gateways, there are presets for use with ttn.

Using the web interface provided by ttn, the implants can be registered using their globally unique DevEUI. All kinds of user application can be created and linked to specific implants using ttn.

For example, python can be used as an efficient programming language for application prototyping. Packets received by any gateway configured for ttn are forwarded to ttn. If the implant is registered for an application, the user application is notified by ttn servers over MQTT (Message Queuing Telemetry Transport). The application receives all payload data of the radio packet, as well as meta data like RSSI, timestamp and location of the gateway the packet was received by. The application then can process the data to visualize sensor readings or store the data in a database for future evaluation. Ideally, a user-friendly application would provide a web interface that can be used to plot the implants readings, export data and configure the implants settings like sample rate and electrode configuration using a web browser.

# 7 Implant Tests and Results

## 7.1 LoRa Range Test

To test the range of the implant's radio link, the LoRaWAN gateway was placed on an open field and the implant was moved away from it. For this purpose the STM32 in the implant was programmed to send beacon messages to the gateway with a maximum transmission strength of +15 dBm at intervals of 500 ms. A GPS logger was carried together with the implant to later measure the distance between gateway and implant using the timestamps of the beacon messages and GPS positions. The test was performed two times, once with the implant in open air and once in closed hands to simulate about 3 cm of tissue. The implant was always oriented in such a way that the upper sensor opening points to the gateway. The RSSI (Received Signal Strength Indicator) reported by the gateway was used as a measure for link quality.

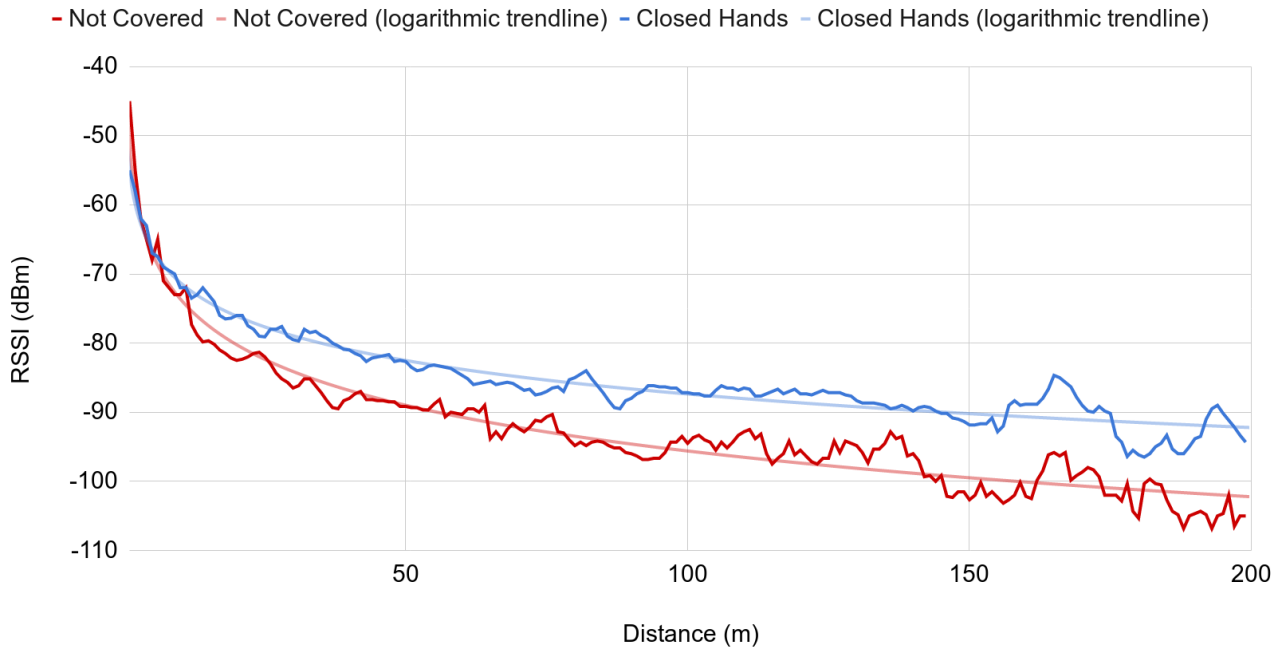


Figure 40: RSSI over distance for both tests.

The RSSI is measured in decibel-milliwatts. It describes the absolute power applied to the input of the receiver, as it is received from the transmitter. A lower value thus means less signal strength.

As seen in [Figure 47](#), the received signal at a given distance is stronger for the sensor covered in hands compared to operation in the open air. This is because the antenna in the implant was designed for a surrounding with high relative permittivity. The low relative permittivity of a surrounding made of air causes an impedance mismatch that is more significant than the additional attenuation caused by the tissue of the hands.

The used gateway can reliably receive data packets with an input power down to -120 dBm. Since the received power for a long distance of 100 m is higher than required, the transmitting power of the LoRa transceiver could be reduced to increase battery lifetime.

The experiment was only carried out for a distance of up to 200 m, as the RSSI fluctuates more and more due to multipath propagation for larger distances. Successful transmission of packets have been tested for a distance of up to 1000 m.

## 7.2 Power Consumption

Since the battery lifetime is longer than the scope of this thesis, no real lifetime test can be performed. Instead, to estimate the expected lifetime and to get a reference for configuring measurement settings, the power consumption of all functions of the implant have been measured using a Yokogawa GS610 sourcemeter. For this a battery with a voltage of 2.7V was used.

Mode	STM32	Analog front-end	Radio
Standby	8.3 $\mu\text{A}$ (0.022 mW)	0.8 $\mu\text{A}$ (0.002 mW)	0.16 $\mu\text{A}$ (0.0004 mW)
Measuring	392 $\mu\text{A}$ (1.06 mW)	478 $\mu\text{A}$ (1.29 mW)	0.16 $\mu\text{A}$ (0.0004 mW)
Transmitting	376 $\mu\text{A}$ (1.02 mW)	0.8 $\mu\text{A}$ (0.002 mW)	39.7 mA (107.2 mW)

Given the operating schedule in [Figure 39](#), it is possible to calculate the expected battery lifetime in days:

$$\text{days} = \frac{210\text{mAh} \cdot \frac{1}{24\text{h}}}{\frac{(8.3\mu\text{A}+0.8\mu\text{A}+0.16\mu\text{A}) \cdot (60\text{s}-n \cdot T_m - T_{tx})}{60\text{s}}} + \frac{(392\mu\text{A}+478\mu\text{A}+0.16\mu\text{A}) \cdot n \cdot T_m}{60\text{s}} + \frac{0.376\mu\text{A}+0.8\mu\text{A}+39.7\text{mA} \cdot T_{tx}}{60\text{s}} \quad (7.1)$$

With  $n$  being the chosen amount of measurements per minute performed (sample rate),  $T_m = 1$  s,  $T_{tx} = 22$  ms and a battery capacity of 210 mAh.

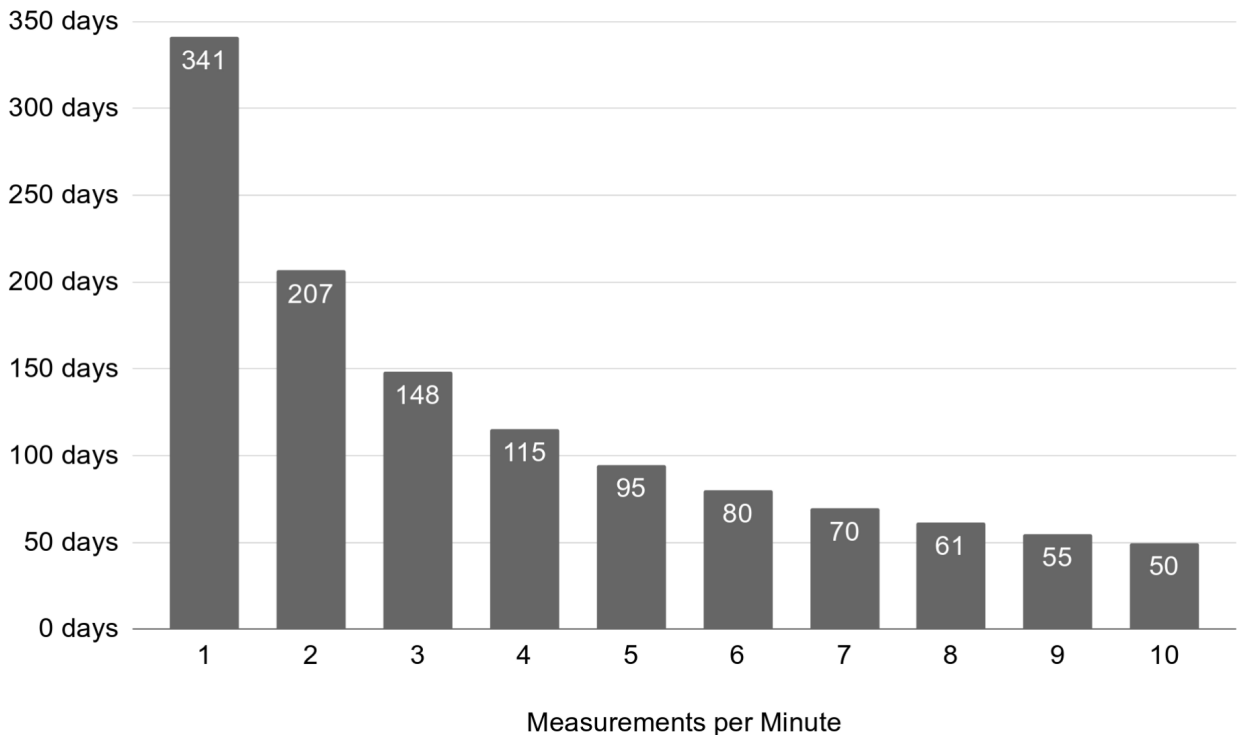


Figure 41: Extrapolated battery lifetime over sample rate.

Since the AFE requires much power and operates for a significant amount of time, the sample rate has a big influence on the expected battery lifetime. With the AFE permanently disabled, the implant could operate for up to two years, while measuring every 6 seconds reduces lifetime to 50 days. It is thus important to select a suitable sample rate if long battery lifetime is required.

### 7.3 Leakage Test

In order to test the tightness of the seal between ISFET dies and the implants package, the leakage current between electrolyte and the ISFET's drain, i.e. an electrically insulated part of the sensor, was measured over a period of 24 hours for each design iteration. One implant half equipped with a sensor board is clamped into a 3D printed holder, with which a microfluidic attachment with inlet and outlet can be pressed onto the sensor opening. Fresh electrolyte flows slowly (10 ml / h) by gravity from a high vessel to a lower placed vessel. A voltage of 3 V is applied between electrolyte and sensor via the electrically conductive electrolyte, tap water. This corresponds to typical operating voltage of the sensor. The current that flows through the electrolyte through potential leak paths to the isolated contacts of the sensor is measured via an amperemeter against ground.

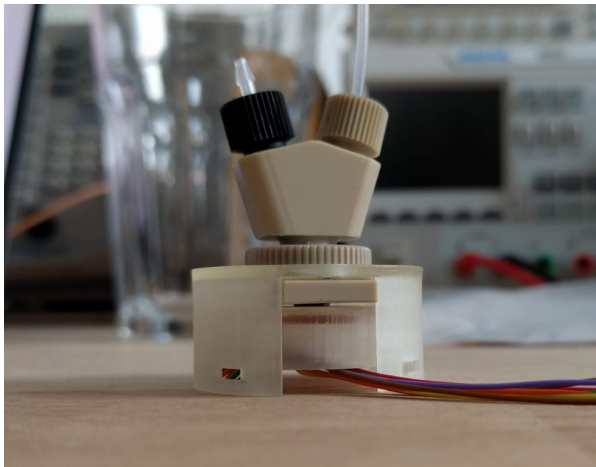


Figure 42: Implant holder with microfluidic attachment for leakage stress test. Photo created by author.

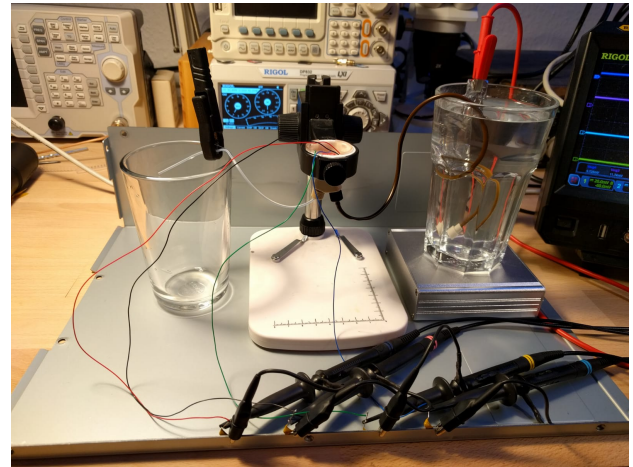


Figure 43: Measurement setup. Right is fresh electrolyte, left is waste water. Photo created by author.

Since the impedance of the leak path is very high, no high requirements are placed on the internal resistance of the measuring device. Thus a Rigol MSO5354 oscilloscope with 1 M $\Omega$  internal resistance was used. This has the advantage that the measurement data on up to four channels / electrodes can easily be logged on a computer using LAN eXtensions for Instrumentation (LXI). A measured voltage of 1 mV therefore corresponds to a leakage current of 1 nA with a maximum error of 3% [45].

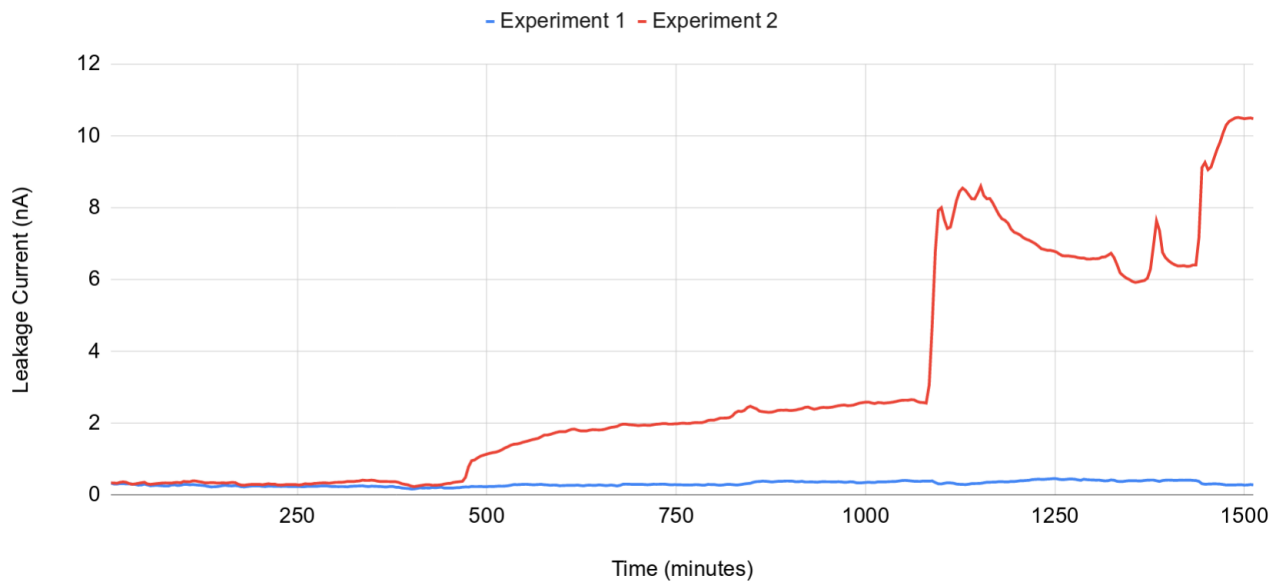


Figure 44: Leakage current of two implant versions in comparison.

Figure 44 shows two leakage current curves recorded independently of each other for the measurement setup described above. Experiment 1 is the final development stage, with resin-printed housing. Experiment 2 is of an early development stage, where the dimensions of the mandrel for the o-ring were not optimal.

While the leakage current for experiment 2 is within the expected leakage current of less than 1 nA (0.309 nA) for the first 7h, it increases slowly after 7.5h until a final leakage current of 10.5 nA is measured after a sudden jump towards the end of the measurement period. Probably the seal between the o-ring and the housing failed here, which caused moisture to slowly penetrate the FR4 PCB board material until there was a good electrical connection between the sensor contacts and the electrolyte.

In experiment 1 the leakage current is initially at 0.309 nA, after 24h it measures 0.28 nA. A final leakage current of 0.295 nA was also measured in a further test over a period of 72 hours. It can therefore be expected that this packaging is initially leak-proof and meets the requirements for the implant.

In further studies, stress tests have to be conducted to simulate long-time aging with actual PEEK housing and under special conditions like phosphate buffered saline at elevated temperature.

## 7.4 Sensor Implant Operation Test

This test requires all components described in this thesis to work properly. Because the sensor design can only measure differential pH, the implant was placed inside a beaker filled with slightly acidic water with pH of 6 (distilled water plus some pH 4 buffer to add ions). Then a few drops of pH 9 buffer (blue) were placed on the top of the implant, so it would cover the sensor opening and get in touch with the upper ISFET. This causes a pH drift from top to bottom that slightly decreases over time as the pH buffer is diluted by entropy.



Figure 45: Implant in test solution after 10 min. Photo created by author.



Figure 46: Implant in test solution after 60 min. Photo created by author.

The ISFETS were operated at a drain-source current of  $80 \mu\text{A}$ . The gate electrode was programmed to a voltage of  $3\text{V}$ . The big ring electrode was left floating. The measured gate-source threshold voltage of each ISFET was send to the LoRa gateway, as well as temperature and status information on the AFE.

Since the relation between threshold voltage and pH is directly proportional, the pH difference can be calculated using this formula:

$$\Delta\text{pH} = \frac{U_{\text{th}}(\text{upper}) - U_{\text{th}}(\text{lower})}{\alpha \cdot 0.0591V} \quad (7.2)$$

With  $\alpha$  being the ISFET sensitivity factor of 0.964.

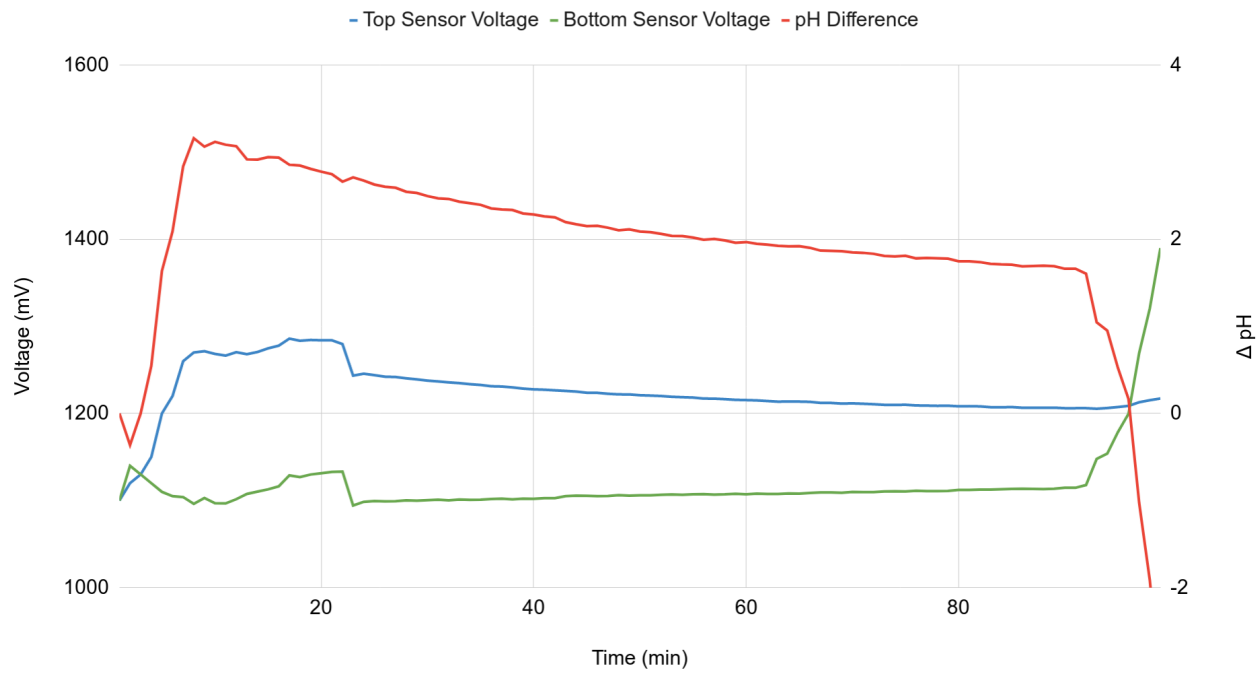


Figure 47: Differential pH as measured by the implant over time.

Both ISFET sensors start off at an equivalent threshold voltage. The pH 9 buffer was added after 1 minute, causing a pH gradient that has it's maximum after 10 minutes with a delta of 3.6 pH steps. As the pH buffer slowly dilutes, the upper sensor voltage decays while the lower voltage slowly rises. Though the absolute pH of the solution increased, once fully mixed, the difference between upper and lower sensor should return to zero.

Between 10 min and 25 min after adding the buffer, the readings of both ISFET sensors show unexpected behaviour, notably the rapid drop in readout voltage at minute 23. This is likely due to the unpredictable behaviour of the on-chip platinum pseudo-reference electrode. Since the same electrode is used for both sensors, this affects both reading, and the calculated difference shows only little distortion.

Originally, the experiment was supposed to run for several hours, ideally until to a point where the pH buffer was fully diluted so both ISFETs measure the same pH. The experiment was stopped after 90 minutes as the bottom sensor apparently broke. It is unknown what caused the defect, but since the other sensor is also slightly affected by the fault, it is likely that the seal broke and current leaked into the electrolyte, disturbing the nearby but also the opposite sensor. Further investigation and tests on the sealing are required.

## 8 Outlook

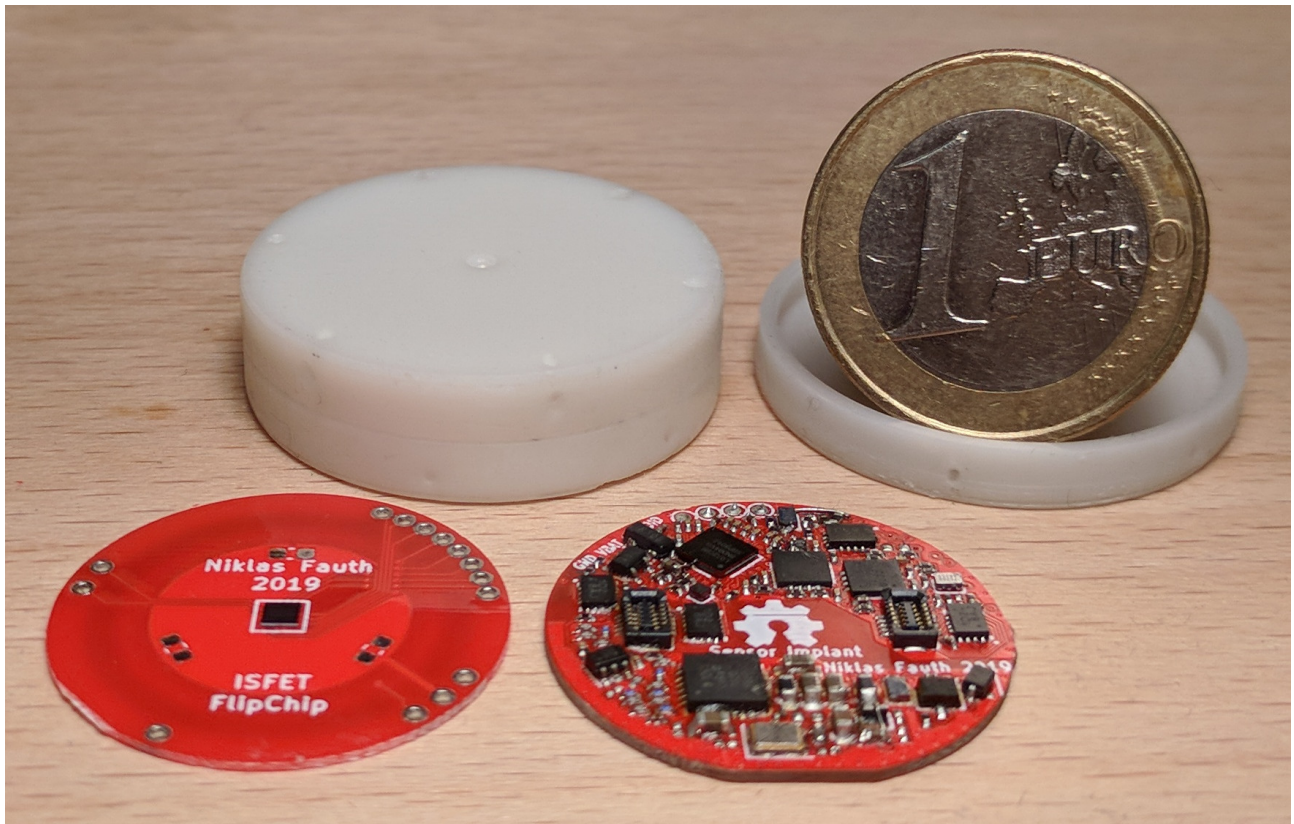


Figure 48: Assembled Implant with mainboard & sensor PCB, 1 Euro coin for size reference.  
Photo created by author

In the context of this work, an implant was developed to be used in animal experiments in cancer research. However, it is still a prototype. The concept has not been proven to fulfill all of the requirements for use in animals or even humans:

The focus of this work was particularly on the development and manufacture of the implant. For the further use of this design, additional tests like biocompatibility of the used materials and long-term leakage test are necessary to find weak points and identify possible problems.

Materials were used for the purpose of rapid prototyping that do not meet the requirements of USP Class VI and therefore must not be used in the body. For example, the epoxy used to seal the implant is not yet suitable for medical application and would have to be replaced in an actual application.

Following this work, up to ten of the implants described in this thesis will be assembled for further testing. This will also serve as a trial of how well the design is suited to be produced in larger quantities. The experience gained from this small series will help to further optimize the design in this respect.

In the longer term, the next generation of the ISFET sensor will improve by integrating more electronics and intelligence into the chip. So far, this part of electronics is the largest area on the mainboard, mainly because there was little potential for integration with existing IC solutions due to this special application. While the current ISFET chip contains only the ISFET and

REFFET transistors, the analog circuit for operating and biasing the ISFET, as well as the multiplexer to select the individual ISFET sensors, will be integrated in the future.

Due to the high demand for LoRa radio ICs, it is to be expected that products will be available in the near future that integrate a microcontroller into a LoRa transceiver. So far, this only exists as a PCB module, the realization as a single IC could save a lot of space.

Together with the developments of the ISFET sensor, the entire electronics of the implant could be reduced from the current 12 ICs to only 2 or 3 ICs. This would allow an overall reduction of the implants volume by more than half, or potential for increasing battery capacity.

## References

- [1] S. Becker, Y. Eminaga, D. Hofsöy, J. Clauss, M. Sattler, B. Wolf, "Intelligent implants for monitoring the hypoxia status of tissue", *BMT 2010; 55 (Suppl 1) pp.4-5*, 2010.
- [2] W.H. Baumann, M. Lehmann, A. Schwinde, R. Ehret, M. Brischwein, B. Wolf, "Micro-electronic sensor system for microphysiological applicationon living cells", 1999.
- [3] D. A. Yardley, "Drug Resistance and the Role of Combination Chemotherapy in Improving Patient Outcomes", 2013. doi: [10.1155/2013/137414](https://doi.org/10.1155/2013/137414).
- [4] K. M. Wolf B, "pH-abhängige Selbstorganisation von Tumorwachstum und Invasion", 1995.
- [5] D. R. A. Covington A. K. Bates R. G., "Definitions of pH scales, standard reference values, measurement of pH, and related terminology", 1985. doi: [10.1351/pac198557030531](https://doi.org/10.1351/pac198557030531).
- [6] S. Z. Chen M. Chen C., "Extracellular pH is a biomarker enabling detection of breast cancer and liver cancer using CEST MRI", 2017. doi: [10.18632/oncotarget.17404](https://doi.org/10.18632/oncotarget.17404).
- [7] R. H. Wike-Hooley J.L. Haveman J., "The relevance of tumour pH to the treatment of malignant disease", 1984. doi: [10.1016/S0167-8140\(84\)80077-8](https://doi.org/10.1016/S0167-8140(84)80077-8).
- [8] Z. Yi and J. Sayago, "Transistors as an Emerging Platform for Portable Amplified Biodection in Preventive Personalized Point-of-Care Testing", 2017, <https://api.intechopen.com/media/chapter/54564/media/F2.png>. doi: [10.5772/67794](https://doi.org/10.5772/67794).
- [9] C. Toumazou and P. Georgiou, "Piet bergveld-40 years of ifset technology: From neuronal sensing to dna sequencing", *Electronics Letters*, vol. 47, S7–S12, Dec. 2011. doi: [10.1049/el.2011.3231](https://doi.org/10.1049/el.2011.3231).
- [10] J. Gordon Betts, Peter Desaix, Eddie Johnson, Jody E. Johnson, Oksana Korol, Dean Kruse, Brandon Poe, James A. Wise, Mark Womble, Kelly A. Young, "Anatomy and Physiology", Chapter 17.9,
- [11] Scientific Animations Inc., *Pancreatic cancer*, <http://www.scientificanimations.com/wiki-images/>  
Modified by author as permitted by the Creative Commons Attribution-Share Alike 4.0 International License, Jan. 2018.
- [12] Zeng FG, Rebscher S, Harrison W, Sun X, Feng H., "Cochlear implants: system design, integration, and evaluation", 2008. doi: [0.1109/RBME.2008.2008250](https://doi.org/10.1109/RBME.2008.2008250).
- [13] H. De Silva, S. Lakmal, P. Chamikara, I. Gunawardana, and D. Chandima, "Qi compliant wireless charging and communication for implantable devices", Sep. 2018, pp. 177–183. doi: [10.1109/EECon.2018.8541001](https://doi.org/10.1109/EECon.2018.8541001).
- [14] M. A. Rothfuss, N. Franconi, J. V. Unadkat, M. L. Gimbel, A. STAR, M. Mickle, and E. Sejdic, "A system for simple real-time anastomotic failure detection and wireless blood flow monitoring in the lower limbs", *IEEE Journal of Translational Engineering in Health and Medicine*, vol. 4, pp. 1–15, Aug. 2016. doi: [10.1109/JTEHM.2016.2588504](https://doi.org/10.1109/JTEHM.2016.2588504).
- [15] E. S. X.J. Fan, *Moisture Sensitivity of Plastic Packages of IC Devices*. 2010, pp. 58–59. doi: [10.1007/978-1-4419-5719-1](https://doi.org/10.1007/978-1-4419-5719-1).
- [16] "Etch Rates for Micromachining Processing — Part II", 2003. doi: [10.1109/JMEMS.2003.820936](https://doi.org/10.1109/JMEMS.2003.820936).
- [17] "NXP "Wafer-level chip-scale package (fan-in WLP and fan-out WLP)"Application Note", <https://www.nxp.com/docs/en/application-note/AN10439.pdf>.
- [18] *Used Epoxy datasheet*, [http://www.uhu-profi.de/uploads/ttx\\_ihtdatasheets/tds\\_plus\\_schnellfest.pdf](http://www.uhu-profi.de/uploads/ttx_ihtdatasheets/tds_plus_schnellfest.pdf).

- [19] “All About Batteries, Part 6: Zinc-Air”,  
[http://www.eetimes.com/author.asp?section\\_id=36&doc\\_id=1321938](http://www.eetimes.com/author.asp?section_id=36&doc_id=1321938).
- [20] “Li/CFx Batteries: The Renaissance”,  
<https://www.sdle.co.il/wp-content/uploads/2018/08/li-cfx-the-renaissance.pdf>.
- [21] “Energizer’s Lithium Iron Disulfide – The best of all worlds for the most demanding applications”,  
<https://www.sdle.co.il/AllSites/810/Assets/energizerisraelpowersourcesmarplenn-ver1.pdf>.
- [22] “Lithium Battery Technologies”,  
<http://www.epectec.com/batteries/lithium-battery-technologies.html>.
- [23] *Ansmann AA – NiMH 2700mAh datasheet*,  
<http://datasheet.octopart.com/5030852-Ansmann-datasheet-5400527.pdf>.
- [24] *muRata CR2032W datasheet*,  
<https://www.mouser.de/datasheet/2/281/R2032W-1372150.pdf>.
- [25] *muRata CR2050W datasheet*,  
<https://www.mouser.de/datasheet/2/281/R2050W-1372159.pdf>.
- [26] *Hirose DF37NC-10DS datasheet*,  
<https://datasheet.lcsc.com/szlcsc/Hirose-HRS-DF37NC-10DS-0-4V-51-C324718.pdf>.
- [27] J.-H. Cho and S. Hyo Woo, “Communication Strategies for Various Types of Swallowable Telemetry Capsules”, in. Oct. 2011, ISBN: 978-953-307-415-3. DOI: [10.5772/23924](https://doi.org/10.5772/23924).
- [28] *Microsemi ZL70323MNJ Datasheet*,  
[https://www.microsemi.com/document-portal/doc\\_download/135307-zl70323-datasheet](https://www.microsemi.com/document-portal/doc_download/135307-zl70323-datasheet).
- [29] *Linx ANT-868-USP datasheet*,  
<https://www.mouser.de/datasheet/2/238/ANT-868-uSP-datasheet%20121228-1175020.pdf>.
- [30] *SiLabs AN782: 868-MHz Antenna Matrix Measurement Reports*,  
<https://www.silabs.com/documents/public/application-notes/AN782.pdf>.
- [31] *Texas Instruments CC1312R Datasheet*,  
<http://www.ti.com/lit/gpn/cc1312r>.
- [32] *HopeRF RFM69CW Datasheet*,  
<https://www.hoperf.com/data/upload/portal/20190307/RFM69CW-V1.1.pdf>.
- [33] *Semtech SX1261 Datasheet*,  
[https://www.semtech.com/uploads/documents/DS\\_SX1261-2\\_V1.1.pdf](https://www.semtech.com/uploads/documents/DS_SX1261-2_V1.1.pdf).
- [34] “ERC Recommendation, 70-03, for SRD860”,  
<https://www.ecodocdb.dk/download/25c41779-cd6e/Rec7003e.pdf>.
- [35] “LoRa Modulation Basics”,  
<https://www.semtech.com/uploads/documents/an1200.22.pdf>.
- [36] V. Mohan, “10 Things About LoRaWAN NB-IoT”,  
<https://blog.semtech.com/title-10-things-about-lorawan-nb-iot>.
- [37] D.Batulzii,  
<http://www.sanchirtech.com/>.
- [38] “LoRa Server, open-source LoRaWAN network-server”,  
<https://www.loraserver.io/>.
- [39] *SX1261 Application Note: Reference Design Explanation*,  
[https://www.semtech.com/uploads/documents/AN1200.40\\_SX1261-2\\_Reference\\_Design\\_Explanation\\_V1.1.pdf](https://www.semtech.com/uploads/documents/AN1200.40_SX1261-2_Reference_Design_Explanation_V1.1.pdf).

## REFERENCES

---

- [40] B. C., *RF Circuit Design*. 1982.
- [41] K. B., “Quality Factor, Bandwidth, and Harmonic Attenuation of Pi Networks”, 2015.
- [42] Wen-Yaw Chung, Febus Reidj G. Cruz, Chung-Huang Yang, Fu-Shun He, Tai-Tsun Liu, Dorota G. Pijanowska, Wladyslaw Torbicz, Piotr B. Grabiec and Bohdan Jarosewicz, “CMOS Readout Circuit Developments for Ion Sensitive Field Effect Transistor Based Sensor Applications”, 2010.
- [43] *Application note AN2834: How to get the best ADC accuracy in STM32 microcontrollers*, [https://www.st.com/content/ccc/resource/technical/document/application\\_note/group0/3f/4c/a4/82/bd/63/4e/92/CD00211314/files/CD00211314.pdf](https://www.st.com/content/ccc/resource/technical/document/application_note/group0/3f/4c/a4/82/bd/63/4e/92/CD00211314/files/CD00211314.pdf).
- [44] “Data Rate and Spreading Factor”,  
[https://docs.exploratory.engineering/lora/dr\\_sf/](https://docs.exploratory.engineering/lora/dr_sf/).
- [45] *Rigol MSO5000 datasheet*,  
[https://www.batronix.com/files/Rigol/Oszilloskope/MSO5000/MSO5000\\_DataSheet\\_EN.pdf](https://www.batronix.com/files/Rigol/Oszilloskope/MSO5000/MSO5000_DataSheet_EN.pdf).

## Appendix

Additional design files such as PCB layouts and CAD models of components can be found at  
<https://github.com/NiklasFauth/sensor-implant>

All documents are being released under the MIT License:

Copyright (c) 2019 Niklas Fauth

Permission is hereby granted, free of charge, to any person obtaining a copy of this software and associated documentation and design files (the "Design"), to deal in the Design without restriction, including without limitation the rights to use, copy, modify, merge, publish, distribute, sublicense, and/or sell copies of the Design, and to permit persons to whom the Design is furnished to do so, subject to the following conditions:

The above copyright notice and this permission notice shall be included in all copies or substantial portions of the Design.

THE DESIGN IS PROVIDED "AS IS", WITHOUT WARRANTY OF ANY KIND, EXPRESS OR IMPLIED, INCLUDING BUT NOT LIMITED TO THE WARRANTIES OF MERCHANTABILITY, FITNESS FOR A PARTICULAR PURPOSE AND NONINFRINGEMENT. IN NO EVENT SHALL THE AUTHORS OR COPYRIGHT HOLDERS BE LIABLE FOR ANY CLAIM, DAMAGES OR OTHER LIABILITY, WHETHER IN AN ACTION OF CONTRACT, TORT OR OTHERWISE, ARISING FROM, OUT OF OR IN CONNECTION WITH THE DESIGN OR THE USE OR OTHER DEALINGS IN THE DESIGN.

